


In-medium effect on the thermodynamics and transport coefficients in the van der Waals hadron resonance gas

He-Xia Zhang¹ and Jin-Wen Kang¹

*Key Laboratory of Quark & Lepton Physics (MOE) and Institute of Particle Physics,
Central China Normal University, Wuhan 430079, China*

Ben-Wei Zhang^{1*}

*Key Laboratory of Quark & Lepton Physics (MOE) and Institute of Particle Physics,
Central China Normal University, Wuhan 430079, China
and Institute of Quantum Matter, South China Normal University, Guangzhou 510006, China*

 (Received 22 June 2019; revised 18 April 2020; accepted 11 June 2020; published 30 June 2020)

An extension of the van der Waals hadron resonance gas (VDWHRG) model which includes the in-medium thermal modification of hadron masses, the thermal VDWHRG (TVDWHRG) model, is considered in this paper. Based on the 2 + 1 flavor Polyakov linear sigma model (PLSM) and the scaling mass rule of hadrons, we obtain the temperature behavior of all hadron masses for different fixed baryon chemical potentials μ_B . We calculate various thermodynamic observables at $\mu_B = 0$ GeV in the TVDWHRG model. An improved agreement with the lattice data from the TVDWHRG model in the crossover region ($T \sim 0.16$ – 0.19 GeV) is observed as compared to those from the VDWHRG and ideal HRG (IHRG) models. We further discuss the effects of the in-medium modification of hadron masses and VDW interactions between (anti)baryons on the dimensionless transport coefficients, such as the shear viscosity to entropy density ratio (η/s) and scaled thermal (λ/T^2) and electrical (σ_{el}/T) conductivities in the IHRG model at different μ_B by utilizing quasiparticle kinetic theory with relaxation time approximation. We find in contrast to the IHRG model, the TVDWHRG model leads to a qualitatively and quantitatively different behavior of transport coefficients with T and μ_B .

DOI: [10.1103/PhysRevD.101.114033](https://doi.org/10.1103/PhysRevD.101.114033)

I. INTRODUCTION

Strongly interacting matter created in ultrarelativistic heavy-ion experiments at the Relativistic Heavy-Ion Collider of BNL and the Large Hadron Collider of CERN has attracted intense theoretical and experimental investigations. The study of strongly interacting matter can give a deep understanding of the quantum chromodynamics (QCD) phase diagram and equation of state of hot and dense matter. Lattice QCD simulations as a reliable tool to study QCD thermodynamics have demonstrated that at finite temperature and vanishing baryon chemical potential μ_B , there exists a smooth crossover [phase transition from hadronic matter to a chirally symmetric quark-gluon plasma (QGP)] ranging from 0.15 to 0.2 GeV [1,2]. The ideal hadron resonance gas (IHRG) model is a widely used

statistical model which provides a remarkably good description of the lattice QCD data [3–5] at low temperature ($T < 0.15$ GeV) and zero μ_B . However, the IHRG model fails to fit the lattice QCD data in the crossover region ($T = 0.16$ – 0.19 GeV). So, an extended IHRG model called the van der Waals hadron resonance gas (VDWHRG) model, which includes both the long-distance attractive and short-distance repulsive van der Waals–(VDW) type interactions between (anti)baryons, is implemented [6,7]. The results of the thermodynamic quantities within the VDWHRG model are closer to the lattice QCD data in the crossover region than that within the IHRG model.

The transport properties of strongly interacting matter play a significant role in describing the dynamical evolution of hot and dense matter. Shear viscosity for the hadronic sector has been analytically calculated in the relativistic kinetic theory using the Chapman-Enskog (CE) approximation [8–13] and relaxation time approximation (RTA) [14–17]. In Ref. [18], shear viscosity for pion gas has been obtained in the linear response theory using Kubo formulas. The shear viscosity for the hadronic phase has also been computed in the microscopic transport model (e.g., SMASH [19], the ultrarelativistic quantum molecular

*bwzhang@mail.ccnucnu.edu.cn

Published by the American Physical Society under the terms of the Creative Commons Attribution 4.0 International license. Further distribution of this work must maintain attribution to the author(s) and the published article's title, journal citation, and DOI. Funded by SCOAP³.

dynamics (UrQMD) model [20], B3D transport model [21], and PHSD [22]), excluded volume HRG (EVHRG) model [23–25], chiral perturbative theory (ChPT) [26–28], effective QCD models [29–32], quasiparticle theory [33,34], scaled hadron mass-couplings (SHMC) model [35], and so on. A few articles also deal with electrical conductivity in pure pion gas [27,36]. In hadronic matter, electrical conductivity has been estimated by employing the relativistic kinetic theory [37,38] and Kubo formalism [39]. Furthermore, electrical conductivity in the hadronic temperature domain was also recently computed in the transport code SMASH [40] in the PHSD transport model [41,42] in anisotropic lattice QCD simulation [43]. Another important transport coefficient is thermal conductivity which has been calculated in hot pion gas [14,15,44–46] and a hadronic gas mixture [12,47,48] using kinetic theory. Recently, the electrical and thermal conductivities of the hadronic temperature domain have also been estimated in effective QCD models [29,49,50] and the EVHRG model [51]. However, so far most of these calculations have taken the vacuum hadron masses as inputs and have not taken into account the influence of in-medium hadron masses on transport coefficients.

As we know, spontaneous chiral symmetry breaking is an important feature in QCD vacuum, which is related to the generation of hadron masses [52–54]. With the increase of temperature or baryon chemical potential, chiral symmetry will be restored, which implies that the masses of constituent quarks should be reduced to zero. Once the constituent quark masses are relevant to the temperature and baryon chemical potential, the masses of the subsequent hadrons should also be naturally dependent on the temperature and baryon chemical potential. In the literature, two main effective QCD-like models, the Polyakov-Nambu-Jona-Lasinio (e.g., [55,56]) and the Polyakov linear sigma model (PLSM) (e.g., [57–61]) are widely used. These models are successful in explaining the dynamics of both chiral-symmetry-breaking restoration and the confinement-deconfinement transition, as well as describing the thermal evolution of meson masses in hot and dense QCD matter. So it is of great interest to replace vacuum hadron masses with temperature- and chemical-potential-dependent masses to explore the thermal hadron mass effect on the thermodynamic quantities and transport coefficients in hot and dense hadronic matter.

In this work, we develop a thermal VDWHRG (TVDWHRG) model, which is an extension of the VDWHRG model by including the dependence of hadron masses on temperature T and baryon chemical potential μ_B . In the TVDWHRG model, we utilize the 2 + 1 flavor PLSM combined with the generalized mass scaling rule of hadrons to obtain the thermal behavior of hadron masses. Then, these thermal hadron masses are taken as dynamic inputs to calculate the thermodynamic quantities in the

VDWHRG model. We further explore how the effects of thermal hadron masses and VDW interactions influence the transport coefficients, such as shear viscosity and electrical and thermal conductivities in hadronic matter. In our model, the derivation of transport coefficients is performed by solving the Boltzmann equation in the relaxation time approximation.

The paper is organized as follows. In Sec. II, we review the ideal and interacting HRG models. In Sec. III, we give a brief overview of the PLSM and discuss the analytical expressions for the medium modifications of hadron masses at finite temperature and baryon chemical potential. In Sec. IV, we present the formulas of the transport coefficients in the quasiparticle kinetic theory under the relaxation time approximation. In Sec. V, the numerical results and discussions are presented. Section VI summarizes our study.

II. HADRON RESONANCE GAS

A. Ideal hadron resonance gas model

In the IHRG model, all thermodynamic quantities can be obtained from the sum of the logarithm of the grand canonical partition function over all hadrons and resonances [62]

$$\ln Z^{\text{id}} = \sum_i \ln Z_i^{\text{id}}(T, \mu_i, m_i). \quad (1)$$

For particle species i ,

$$\ln Z_i^{\text{id}} = \pm \frac{V g_i}{(2\pi)^3} \int d^3 p \ln [1 \pm \exp(-(E_i - \mu_i)/T)]. \quad (2)$$

Here, id refers to the ideal (noninteracting) gas, V is the volume of the system, g_i stands for the degeneracy factor which satisfies the relation $g_i = (2J_i + 1)$, J_i is the angular momentum of hadron species i , and the sign \pm is positive for fermions and negative for bosons. $E_i = \sqrt{p^2 + m_i^2}$ denotes the energy of the single particle. m_i is the mass of hadron species i , which is usually taken as the vacuum hadron mass. In this paper, we also consider the effects of the finite temperature and chemical potential on masses of hadrons. $\mu_i = B_i \mu_B + S_i \mu_S + Q_i \mu_Q$ is the chemical potential of particle species i , where B_i , S_i , Q_i are the baryon number, strangeness, and electric charge, respectively, and $\mu_{B/S/Q}$ gives the corresponding chemical potential. We assume $\mu_S = \mu_Q = 0$, which is a reasonable approximation in heavy-ion collision experiments [63]. The thermodynamic quantities (pressure, energy density, and number density) in the IHRG model can be given by [64,65]

$$P^{\text{id}} = T \frac{\partial \ln Z^{\text{id}}}{\partial V} = \sum_i g_i \int \frac{d^3 p}{(2\pi)^3} \frac{p^2}{3E_i} f_i^{\text{id}}, \quad (3)$$

$$\epsilon^{\text{id}} = -\frac{1}{V} \left(\frac{\partial \ln Z^{\text{id}}}{\partial \frac{1}{T}} \right)_{\frac{\mu_i}{T}} = \sum_i g_i \int \frac{d^3 p}{(2\pi)^3} E_i f_i^{\text{id}}, \quad (4)$$

$$n^{\text{id}} = \frac{T}{V} \left(\frac{\partial \ln Z^{\text{id}}}{\partial \mu_i} \right)_{V,T} = \sum_i g_i \int \frac{d^3 p}{(2\pi)^3} f_i^{\text{id}}, \quad (5)$$

where f_i^{id} is the ideal Fermi or Bose distribution function $f_i^{\text{id}}(T, p, \mu_i) = 1/(\exp[(E_i - \mu_i)/T] \pm 1)$.

B. Interacting hadron resonance gas

In this work, we also consider a more realistic system, where the short-distance repulsive interaction and the long-distance attractive interaction exist among the hadrons. There are different phenomenological excluded-volume models to simulate the repulsive interaction of hadrons, such as the van der Waals [66] and Carnahan-Starling excluded-volume models [67] with the effect of quantum statistics. For the attractive interaction, four forms have been discussed [6,68–70]: the van der Waals, Redlich-Kwong-Soave (RKS), Peng-Robinson (PR), and Clausius models. Therefore, to take into account both the repulsive interaction and attractive interaction, eight interacting hadron resonance gas models could be employed: the VDW, RKS, PR, Clausius, VDW-CS, RKS-CS, PR-CS, and Clausius-Carnahan-Starling (CS) models. In the interacting hadron resonance gas model, the repulsive and attractive interactions only exist between baryon-baryon pairs and between antibaryon-antibaryon pairs while the baryon-antibaryon, meson-baryon, and meson-meson interactions are neglected [6,7]. So, the total pressure in the grand canonical ensemble can be written as [7]

$$P(T, \mu) = P_M(T, \mu) + P_B(T, \mu) + P_{\bar{B}}(T, \mu), \quad (6)$$

with

$$P_M(T, \mu) = \sum_{z \in M} P_z^{\text{id}}(T, \mu_z), \quad (7)$$

$$P_B(T, \mu) = [F(h_B) - h_B F'(h_B)] \sum_{z \in B} P_z^{\text{id}}(T, \mu_z^{B*}) + n_B^2 u'(n_B), \quad (8)$$

$$P_{\bar{B}}(T, \mu) = [F(h_{\bar{B}}) - h_{\bar{B}} F'(h_{\bar{B}})] \sum_{z \in \bar{B}} P_z^{\text{id}}(T, \mu_z^{\bar{B}*}) + n_{\bar{B}}^2 u'(n_{\bar{B}}), \quad (9)$$

where μ is the baryon chemical potential in the current work, and the subscripts M , B , \bar{B} stand for mesons, baryons, and antibaryons, respectively. The constructed functions $F(h_{B(\bar{B})})$ and $u(n_{B(\bar{B})})$ are related to the repulsive and attractive interactions between (anti)baryon pairs,

respectively. The analytical forms of $F(h_{B(\bar{B})})$ and $u(n_{B(\bar{B})})$ are different according to the choice of interacting hadron resonance gas models listed previously. $h_{B(\bar{B})}$ denotes the packing ratio of all (anti)baryonic volume occupied in the total system volume that satisfies the relation $h_{B(\bar{B})} = \frac{b}{4} n_{B(\bar{B})} \cdot n_{B(\bar{B})}$, which is the total number density of (anti)baryons that can be obtained by using $n_B = \partial P_B / \partial \mu_z$,

$$n_B(T, \mu) = F(h_B) \sum_{z \in B} n_z^{\text{id}}(T, \mu_z^{B*}). \quad (10)$$

Additionally, the shifted chemical potential of baryon μ_z^{B*} is given as [7]

$$\mu_z^{B*} - \mu_z = \frac{b}{4} F'(h_B) \sum_{z \in B} P_z^{\text{id}}(T, \mu_z^{B*}) - u(n_B) - n_B u'(n_B). \quad (11)$$

The key is to obtain μ_z^{B*} . At a given T and μ , μ_z^{B*} can be calculated by solving Eqs. (10) and (11) numerically. Accordingly, other thermodynamic quantities such as the entropy density $s_B = (\partial P_B / \partial T)_\mu$ and the energy density can be determined by

$$s_B(T, \mu) = F(h_B) \sum_{z \in B} s_z^{\text{id}}(T, \mu_z^{B*}) \quad (12)$$

and

$$\epsilon_B(T, \mu) = F(h_B) \sum_{z \in B} \epsilon_z^{\text{id}}(T, \mu_z^{B*}) + n_B u(n_B). \quad (13)$$

Equations (10)–(13) are also applicable to antibaryons. In this work, we use the VDW model in which $F(h_{B(\bar{B})}) = 1 - 4h_{B(\bar{B})}$ and $u(n_{B(\bar{B})}) = -an_{B(\bar{B})}$. The parameters a and b are determined by reproducing the properties of nuclear matter in the ground state [71] according to the choice of interacting hadron resonance gas models [72].

III. MASS SENSITIVITY OF HADRONS AT FINITE TEMPERATURE AND BARYON CHEMICAL POTENTIAL

A. The PLSM

As mentioned in Sec. I, the melting behavior of hadron masses is related to the temperature- and chemical-potential-dependent constituent quarks. In the present work, the dynamical information of the constituent quark masses in the QCD medium can be determined by employing the SU(3) PLSM. Next, we briefly introduce the linear sigma model with $N_f = 2 + 1$ flavor quarks coupled to the Polyakov-loop dynamics to formulate the PLSM. The related Lagrangian is given as [57–61]

$$\mathcal{L} = \mathcal{L}_{\text{chiral}} - \mathcal{U}(\phi, \phi^*, T), \quad (14)$$

where the chiral part of the Lagrangian $\mathcal{L}_{\text{chiral}} = \mathcal{L}_{\text{quark}} + \mathcal{L}_{\text{meson}}$ has $SU(3)_L \times SU(3)_R$ symmetry (details can be found in [73]). The first term in $\mathcal{L}_{\text{chiral}}$ corresponds to the fermionic contributions from quarks, and the second term represents the mesonic contribution; both contributions have been extensively discussed in Refs. [58–61]. The second term in Eq. (14), $\mathcal{U}(\phi, \phi^*, T)$, represents the Polyakov-loop effective potential to introduce the gluon degrees of freedom and the dynamics of the quark-gluon interactions [74], which is expressed by using the dynamics of the thermal expectation value of a color traced Wilson loop in the temporal direction. Correspondingly, the traced Polyakov-loop variable and its conjugate can read as

$$\phi = \langle \text{Tr}_c L \rangle / N_c, \quad \phi^* = \langle \text{Tr}_c L^\dagger \rangle / N_c, \quad (15)$$

where L is the Polyakov loop, and L can be represented by a matrix in color space [74]

$$L(\vec{x}) = \mathcal{P} \exp \left[i \int_0^\beta d\tau A_0(\vec{x}, \tau) \right], \quad (16)$$

where $\beta = 1/T$ denotes the inverse temperature, and \mathcal{P} and A_0 are the path ordering and temporal component of the Euclidean vector field, respectively [74]. At vanishing chemical potential $\phi = \phi^*$, the Polyakov loop is recognized as an order parameter for the deconfinement-phase transition. In this work, we use a logarithmically formed Polyakov-loop effective potential [75], which is motivated by the underlying QCD symmetries in the pure gauge limit

$$\frac{\mathcal{U}_{\text{Log}}(\phi, \phi^*, T)}{T^4} = \frac{-a(T)}{2} \phi^* \phi + b(T) \ln[1 - 6\phi^* \phi + 4(\phi^{*3} + \phi^3) - 3(\phi^* \phi)^2], \quad (17)$$

with

$$\begin{aligned} a(T) &= a_0 + a_1(T_0/T) + a_2(T_0/T)^2, \\ b(T) &= b_3(T_0/T)^3. \end{aligned} \quad (18)$$

In Eq. (18), $a_0 = 3.51$, $a_1 = -2.47$, $a_2 = 15.2$, $b_3 = -1.75$, which are determined by fitting pure gauge lattice data [75]. $T_0 = 270$ MeV is the critical temperature for the deconfinement in Yang-Mills theory. In the mean field approximation [60], the grand canonical potential of the PLSM can be written as

$$\Omega(T, \mu_{\text{fl}}) = U(\sigma_x, \sigma_y) + \mathcal{U}(\phi, \phi^*, T) + \Omega_{\bar{q}q}(T, \mu_{\text{fl}}, \phi, \phi^*), \quad (19)$$

where σ_x and σ_y stand for the nonstrange and strange chiral condensates, respectively. The first term in Eq. (19), the purely mesonic potential, is given as

TABLE I. The parameters of the PLSM employed in the present calculation.

c (MeV)	λ_1	m^2 (MeV ²)	λ_2
4807.84	13.49	-(306.26) ²	46.48
h_x (MeV ³)	h_y (MeV ³)	m_σ (MeV)	
(120.73) ³	(336.41) ³	800	

$$\begin{aligned} U &= -h_x \sigma_x - h_y \sigma_y + \frac{m^2(\sigma_x^2 + \sigma_y^2)}{2} - \frac{c \sigma_x^2 \sigma_y}{2\sqrt{2}} \\ &+ \frac{\lambda_1 \sigma_x^2 \sigma_y^2}{2} + \frac{(2\lambda_1 + \lambda_2) \sigma_x^4}{8} + \frac{(\lambda_1 + \lambda_2) \sigma_y^4}{4}. \end{aligned} \quad (20)$$

Here, m^2 , h_x , h_y , λ_1 , λ_2 , and c are model parameters as reported in Ref. [73]. The parameters used in the present work are listed in Table I. The third term in Eq. (19) $\Omega_{\bar{q}q}(T, \mu_{\text{fl}}; \phi, \phi^*)$ is the quark-antiquark potential, which can be shown as [60]

$$\Omega_{\bar{q}q} = -2T \sum_{\text{fl}=u,d,s} \int \frac{d^3 p}{(2\pi)^3} (\ln g_{\text{fl}}^+ + \ln g_{\text{fl}}^-). \quad (21)$$

The expressions of g_{fl}^+ and g_{fl}^- are defined as

$$g_{\text{fl}}^+ = [1 + 3(\phi + \phi^* e^{-E_{\text{fl}}^+/T}) e^{-E_{\text{fl}}^+/T} + e^{-3E_{\text{fl}}^+/T}], \quad (22)$$

$$g_{\text{fl}}^- = [1 + 3(\phi^* + \phi e^{-E_{\text{fl}}^-/T}) e^{-E_{\text{fl}}^-/T} + e^{-3E_{\text{fl}}^-/T}], \quad (23)$$

where $E_{\text{fl}}^\pm = E_{\text{fl}} \mp \mu_{\text{fl}}$, $E_{\text{fl}} = \sqrt{p^2 + m_{\text{fl}}^2}$ is the single particle energy with the flavor-dependent constituent (anti)quark mass m_{fl} . For symmetric quark matter, we take the uniform blind chemical potential, i.e., $\mu_{\text{fl}} \equiv \mu_u = \mu_d = \mu_s = \mu_B/3$ [31,73]. Neglecting the small difference in the masses of light quarks, the m_{fl} for the nonstrange and strange quarks can be given by [76]

$$m_q = g \frac{\sigma_x}{2}, \quad m_s = g \frac{\sigma_y}{\sqrt{2}}. \quad (24)$$

In order to obtain the T and μ_B dependence of order parameters σ_x , σ_y , ϕ , and ϕ^* , we minimize the thermodynamic potential Eq. (19) with respect to these mean variables; i.e.,

$$\left. \frac{\partial \Omega}{\partial \sigma_x} = \frac{\partial \Omega}{\partial \sigma_y} = \frac{\partial \Omega}{\partial \phi} = \frac{\partial \Omega}{\partial \phi^*} \right|_{\text{min}} = 0, \quad (25)$$

where $\sigma_x = \bar{\sigma}_x$, $\sigma_y = \bar{\sigma}_y$, $\phi = \bar{\phi}$, $\phi^* = \bar{\phi}^*$ label the global minimum.

B. Hadron masses

We first present the procedure of calculating the T - and μ_B -dependent masses of the pseudoscalar (π, η, η', K) and scalar (σ, a_0, f_0, κ) mesons in the framework of the PLSM. In the thermal field theory, the scalar and pseudoscalar meson masses are defined by the second derivative of the temperature- and quark-chemical-potential-dependent thermodynamic potential $\Omega(T, \mu_{\bar{n}})$ with respect to corresponding scalar fields $\alpha_{S,x} = \sigma_x$ and pseudoscalar fields $\alpha_{P,x} = \pi_x(x, y = 0, \dots, 8)$, which can be expressed as [73]

$$m_{i,xy}^2 \Big|_T = \frac{\partial^2 \Omega(T, \mu_{\bar{n}})}{\partial \alpha_{i,x} \partial \alpha_{i,y}} \Big|_{\min} = (m_{a,xy}^m)^2 + (\delta m_{a,xy}^T)^2, \quad (26)$$

where \min denotes minimizing the grand potential, and $i = S(P)$ corresponds to the scalar (pseudoscalar) mesons. The first term in Eq. (26) is the vacuum meson mass calculated from the second derivative of the purely mesonic potential. The second term corresponds to the in-medium modification of the meson mass due to the quark-antiquark potential at finite temperature and baryon chemical potential, which can be given as

$$\begin{aligned} (\delta m_{i,xy}^T)^2 &= 3 \sum_{\bar{n}=u,d,s} \int \frac{d^3 p}{(2\pi)^3} \frac{1}{E_{\bar{n}}} \left[(A_{\bar{n}}^+ + A_{\bar{n}}^-) \right. \\ &\quad \times \left(m_{\bar{n},xy}^2 - \frac{m_{\bar{n},x}^2 m_{\bar{n},y}^2}{2E_{\bar{n}}^2} \right) \\ &\quad \left. + (B_{\bar{n}}^+ + B_{\bar{n}}^-) \left(\frac{m_{\bar{n},x}^2 m_{\bar{n},y}^2}{2E_{\bar{n}} T} \right) \right]. \quad (27) \end{aligned}$$

The squared constituent quark mass derivative with respect to the meson field $\alpha_{i,a}$, $m_{\bar{n},a} \equiv \partial m_{\bar{n}}^2 / \partial \alpha_{i,a}$, and with respect to meson fields $\alpha_{i,a} \alpha_{i,b}$, $m_{\bar{n},ab} \equiv \partial m_{\bar{n}}^2 / \partial \alpha_{i,a} \partial \alpha_{i,b}$, can be taken from Table III in Ref. [73]. The notations $A_{\bar{n}}^{\pm}$ and $B_{\bar{n}}^{\pm}$ in Eq. (27) have the following definitions:

$$A_{\bar{n}}^+ = \frac{\phi e^{-E_{\bar{n}}^+/T} + 2\phi^* e^{-2E_{\bar{n}}^+/T} + e^{-3E_{\bar{n}}^+/T}}{g_{\bar{n}}^+}, \quad (28)$$

$$A_{\bar{n}}^- = \frac{\phi^* e^{-E_{\bar{n}}^-/T} + 2\phi e^{-2E_{\bar{n}}^-/T} + e^{-3E_{\bar{n}}^-/T}}{g_{\bar{n}}^-}, \quad (29)$$

and $B_{\bar{n}}^{\pm} = 3(A_{\bar{n}}^{\pm})^2 - C_{\bar{n}}^{\pm}$, where $C_{\bar{n}}^{\pm}$ is defined as

$$C_{\bar{n}}^+ = \frac{\phi e^{-E_{\bar{n}}^+/T} + 4\phi^* e^{-2E_{\bar{n}}^+/T} + 3e^{-3E_{\bar{n}}^+/T}}{g_{\bar{n}}^+}, \quad (30)$$

$$C_{\bar{n}}^- = \frac{\phi^* e^{-E_{\bar{n}}^-/T} + 4\phi e^{-2E_{\bar{n}}^-/T} + 3e^{-3E_{\bar{n}}^-/T}}{g_{\bar{n}}^-}. \quad (31)$$

Then, the squared masses of the four scalar mesons are given as [73]

$$m_{a_0}^2 = (m_{a_0}^m)^2 + (\delta m_{S,11}^T)^2, \quad (32)$$

$$m_{\kappa}^2 = (m_{\kappa}^m)^2 + (\delta m_{S,44}^T)^2, \quad (33)$$

$$\begin{aligned} m_{\sigma}^2 &= m_{S,00}^2 \cos^2 \theta_S + m_{S,88}^2 \sin^2 \theta_S \\ &\quad + 2m_{S,08}^2 \sin \theta_S \cos \theta_S, \quad (34) \end{aligned}$$

$$\begin{aligned} m_{f_0}^2 &= m_{S,00}^2 \sin^2 \theta_S + m_{S,88}^2 \cos^2 \theta_S \\ &\quad - 2m_{S,08}^2 \sin \theta_S \cos \theta_S. \quad (35) \end{aligned}$$

And the four pseudoscalar meson masses are

$$m_{\pi}^2 = (m_{\pi}^m)^2 + (\delta m_{P,11}^T)^2, \quad (36)$$

$$m_K^2 = (m_K^m)^2 + (\delta m_{P,44}^T)^2, \quad (37)$$

$$\begin{aligned} m_{\eta'}^2 &= m_{P,00}^2 \cos^2 \theta_P + m_{P,88}^2 \sin^2 \theta_P \\ &\quad + 2m_{P,08}^2 \sin \theta_P \cos \theta_P, \quad (38) \end{aligned}$$

$$\begin{aligned} m_{\eta}^2 &= m_{P,00}^2 \sin^2 \theta_P + m_{P,88}^2 \cos^2 \theta_P \\ &\quad - 2m_{P,08}^2 \sin \theta_P \cos \theta_P, \quad (39) \end{aligned}$$

where the mixing angles $\theta_{S(P)}$ are given by

$$\tan 2\theta_i = \left(\frac{2m_{i,08}^2}{m_{i,00}^2 - m_{i,88}^2} \right), \quad i = S, P, \quad (40)$$

and $m_{i,00/88/08}^2 = (m_{P,00/88/08}^m)^2 + \delta(m_{P,00/88/08}^T)^2$. The detailed expressions of the vacuum contributions $[(m_{a_0}^m)^2, (m_{\kappa}^m)^2, (m_{\pi}^m)^2, (m_K^m)^2$ and $(m_{i,00/88/08}^m)^2]$ from purely mesonic potential in Eqs. (32)–(39) can be obtained from Refs. [60,73].

Next, for all baryons and other heavier mesons, the dependence of their masses on T and μ_B can be obtained by introducing a generalized scaling rule [77–81], which assumes that hadron masses are linear in the constituent quark masses,

$$\begin{aligned} M_{B/M}(T, \mu_B) &= M_{B/M}(0, 0) + (N_q - N_s) \delta M_q(T, \mu_B) \\ &\quad + N_s \delta M_s(T, \mu_B), \quad (41) \end{aligned}$$

where the subscript B/M stands for a given baryon/meson, and $M_{q/s}$ is the light/strange constituent quark mass. $\delta M_{q/s}$ in Eq. (41) denotes the variation of the constituent quark mass with the temperature and baryon chemical potential. N_q and N_s are the number of total quarks and strangeness content, respectively, in a given hadron. For the open strange hadrons, N_s is simply the number of strange (antistrange) quarks. For hidden strange mesons, $N_s = 2/3$ for the flavor singlet and $N_s = 4/3$ for the flavor octet. However, we bear in mind that this approach of obtaining

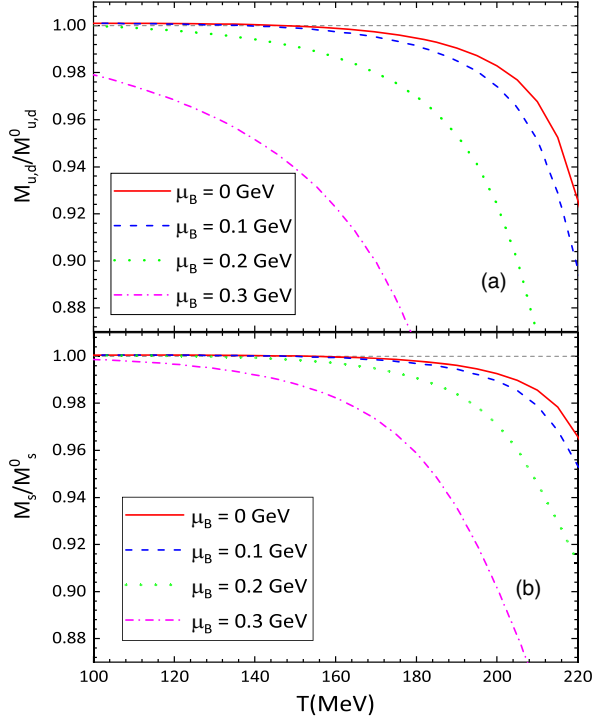


FIG. 1. (a) The temperature dependence of the normalized light (u, d) constituent quark mass ($M_{u,d}/M_{u,d}^0$) for $\mu_B = 0$ (red solid line), 0.1 GeV (blue dashed line), 0.2 GeV (green dotted line), and 0.3 GeV (purple dash-dotted line). (b) The temperature dependence of the normalized strange constituent quark mass (M_s/M_s^0) for different μ_B . The light and strange vacuum constituent quark masses are taken as $M_{u,d}^0 = 300$ MeV and $M_s^0 = 433$ MeV [73], respectively, in the PLSM.

the thermal hadron masses is sketchy and still needs improvement in the future. Figure 1 shows the normalized light constituent quark mass $M_{u,d}/M_{u,d}^0$ and the normalized strange constituent quark mass M_s/M_s^0 as a function of T for different fixed μ_B in the PLSM. The temperature behavior of the normalized constituent quark mass shows a smoothly decreasing feature. The initial temperature at which the light/strange constituent quark masses begin to melt is $T \sim 160/180$ MeV (not the chiral pseudocritical temperature) for $\mu_B = 0$ GeV. As μ_B grows, $M_{u,d/s}/M_{u,d/s}^0$ begins to decrease at smaller temperature, and the decreasing feature of the constituent quark masses becomes more prominent.

Figure 2 shows the temperature and baryon chemical potential dependences of the pseudoscalar mesons (π, K, η', η) and scalar mesons (a_0, κ, σ, f_0) in the PLSM. The masses of these states degenerate at $T \sim 160$ MeV for the $\mu_B = 0$ and 0.1 GeV cases. For the $\mu_B = 0.2$ and 0.3 GeV cases, these states degenerate at $T \sim 130$ MeV and $T < 100$ MeV, respectively. Therefore, the melting behavior of the hadron masses can quantitatively affect the thermodynamic quantities and transport coefficients of hadronic matter, which will be seen later in Sec. V.

IV. TRANSPORT COEFFICIENTS

The transport coefficients in the medium composed of quasiparticles whose masses depend on the temperature and chemical potential can be derived by utilizing the relativistic kinetic theory under the relaxation time approximation [32,82,83]. The general expressions of shear viscosity (η), electrical conductivity (σ_{el}), and thermal conductivity (λ) can be written as [32,82]

$$\eta = \frac{1}{15T} \sum_i g_i \int \frac{d^3 p}{(2\pi)^3} \frac{p^4}{E_i^2} \tau_i f_i^{\text{id}} (1 \pm f_i^{\text{id}}), \quad (42)$$

$$\sigma_{\text{el}} = \frac{1}{3T} \frac{4\pi}{137} \sum_i g_i e_i^2 \int \frac{d^3 p}{(2\pi)^3} \frac{p^2}{E_i} \tau_i f_i^{\text{id}} (1 \pm f_i^{\text{id}}), \quad (43)$$

$$\lambda = \left(\frac{w}{n_B T} \right)^2 \sum_i g_i \int \frac{d^3 p}{(2\pi)^3} \frac{p^2}{3E_i^2} \tau_i \left(B_i - \frac{n_B E_i}{w} \right)^2 \times f_i^{\text{id}} (1 \pm f_i^{\text{id}}). \quad (44)$$

Here, e_i and B_i are the electric charge and baryon number of hadron species i , respectively. w is the total enthalpy density. The sign \pm corresponds to bosons and fermions, respectively. τ_i is the thermal relaxation time of hadron species i . We assume only elastic scattering between hadrons, so the inverse relaxation time τ_i^{-1} for the collision process of $i(p_1) + j(p_2) \rightarrow i(p_3) + j(p_4)$ can be given by [84]

$$\tau_i^{-1} = \sum_j \frac{g_j}{1 + \delta_{ij}} \int \prod_{k=2}^4 \frac{d\Gamma_k}{2E_k} (2\pi)^4 \delta^4(P_{\text{tot}}) |\bar{M}|^2 f_j(p_2), \quad (45)$$

where $d\Gamma_k = d^3 p_k / (2\pi)^3 / (2E_k)$, $\delta^4(P_{\text{tot}}) = \delta^3(p_1 + p_2 - p_3 - p_4) \delta(E_1 + E_2 - E_3 - E_4)$, and the factor $1/(1 + \delta_{ij})$ is to avoid double counting for identical incoming particle species. In Eq. (45), the average of the initial degeneracy factor and the sum of the final degeneracy factor are implicitly included in the matrix element (\bar{M}). Using the formula of the scattering cross section [85]

$$\sigma_{ij} = \frac{\int \prod_{k=3}^4 d\Gamma_k (2\pi)^4 \delta^4(P_{\text{tot}}) |\bar{M}|^2}{4\sqrt{(P_1 \cdot P_2)^2 - m_i^2 m_j^2}} \quad (46)$$

with four-momentum $P_{1(2)} = (E_{1(2)}, p_{1(2)})$, we can then rewrite τ_i^{-1} and take the thermal averaging

$$\tau_i^{-1} \equiv \sum_j \frac{n_j}{1 + \delta_{ij}} \langle \sigma_{ij} v_{ij} \rangle, \quad (47)$$

where $n_j = g_j \int d^3 p_2 / (2\pi)^3 f_j(p_2)$ is the number density of particle species j . It is important to note that if particle

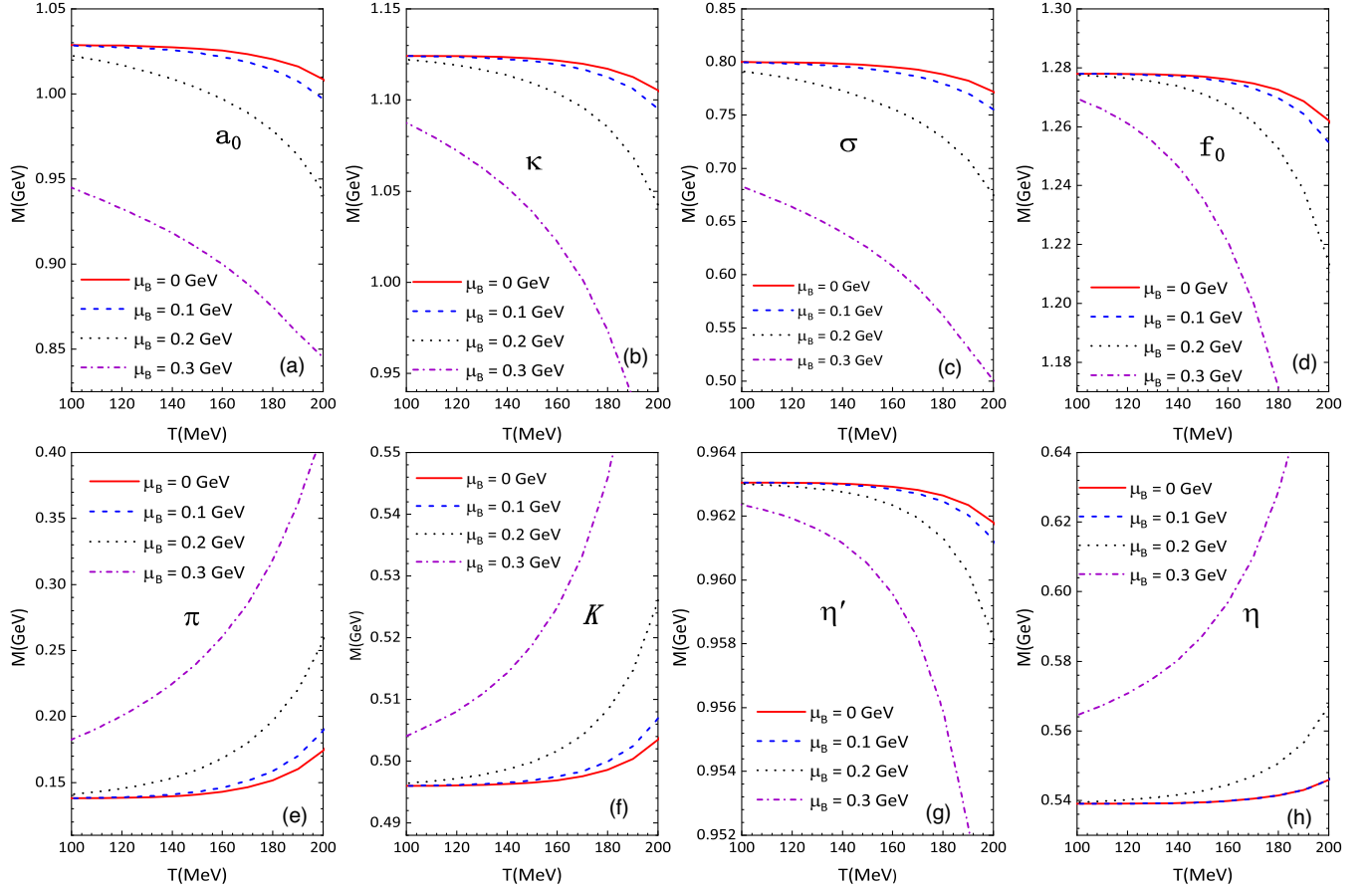


FIG. 2. The temperature dependences of the scalar mesons a_0 , [diagram (a)] κ , [diagram (b)] σ , [diagram (c)] f_0 , and [diagram (d)] the pseudoscalar mesons π , [diagram (e)] K , [diagram (f)] η' , [diagram (g)] η [diagram (h)] at $\mu_B = 0$ GeV (solid red lines), 0.1 GeV (dashed blue lines), 0.2 GeV (dotted black lines), and 0.3 GeV (dotted-dashed purple lines) in the framework of the PLSM.

species j is a baryon/antibaryon, the detailed form of the number density can be modified in the van der Waals hadron resonance gas,

$$n_j(T, \mu_j) = \begin{cases} n_j^{id}(T, \mu_j), & \text{in ideal HRG;} \\ F(h_{B(\bar{B})})n_j^{id}(T, \mu_j^{B(\bar{B})*}), & \text{in VDW HRG.} \end{cases} \quad (48)$$

The Lorentz scalar flow factor is defined as

$$v_{ij} = \frac{\sqrt{(P_1 \cdot P_2)^2 - m_i^2 m_j^2}}{E_1 E_2}. \quad (49)$$

Therefore, the thermal average cross section with the Maxwell-Boltzmann distribution approximation after some uncomplicated simplification can be written as the following form:

$$\begin{aligned} \langle \sigma_{ab} v_{ij} \rangle &= \frac{\int d^3 p_1 d^3 p_2 f_i^{id}(p_1) f_j^{id}(p_2) \sigma_{ij} v_{ij}}{\int d^3 p_1 d^3 p_2 f_i^{id}(p_1) f_j^{id}(p_2)} \\ &= \frac{\int d^3 p_1 d^3 p_2 e^{-E_1 \beta} e^{-E_2 \beta} \sigma_{ij} v_{ij}}{\int d^3 p_1 d^3 p_2 e^{-E_1 \beta} e^{-E_2 \beta}} \\ &= \frac{\beta \int_{S_0}^{\infty} \sigma_{ij} \gamma(S) K_1(\beta \sqrt{S}) \frac{1}{2\sqrt{S}} dS}{4m_i^2 m_j^2 K_2(\beta m_i) K_2(\beta m_j)}, \end{aligned} \quad (50)$$

where \sqrt{S} is the center-of-mass energy, $S_0 = (m_i + m_j)^2$, and $\gamma(S) = [S - (m_i + m_j)^2][S - (m_i - m_j)^2]$. K_n is the modified Bessel function of order n . In this work, we regard all hadrons as hard spheres which have the same radius r_h as nucleons, so σ_{ij} is a constant with $\sigma_{ij} = 4\pi r_h^2$.

V. NUMERICAL RESULTS AND DISCUSSION

In the following, we consider an extension of the VDWHRG model by including thermal evolution of hadron masses, and refer to this new model as the TVDWHRG model. In the treatment of the HRG model, we include all hadrons and resonances up to 2.0 GeV listed by the Particle Data Group [86]. The VDW model yields

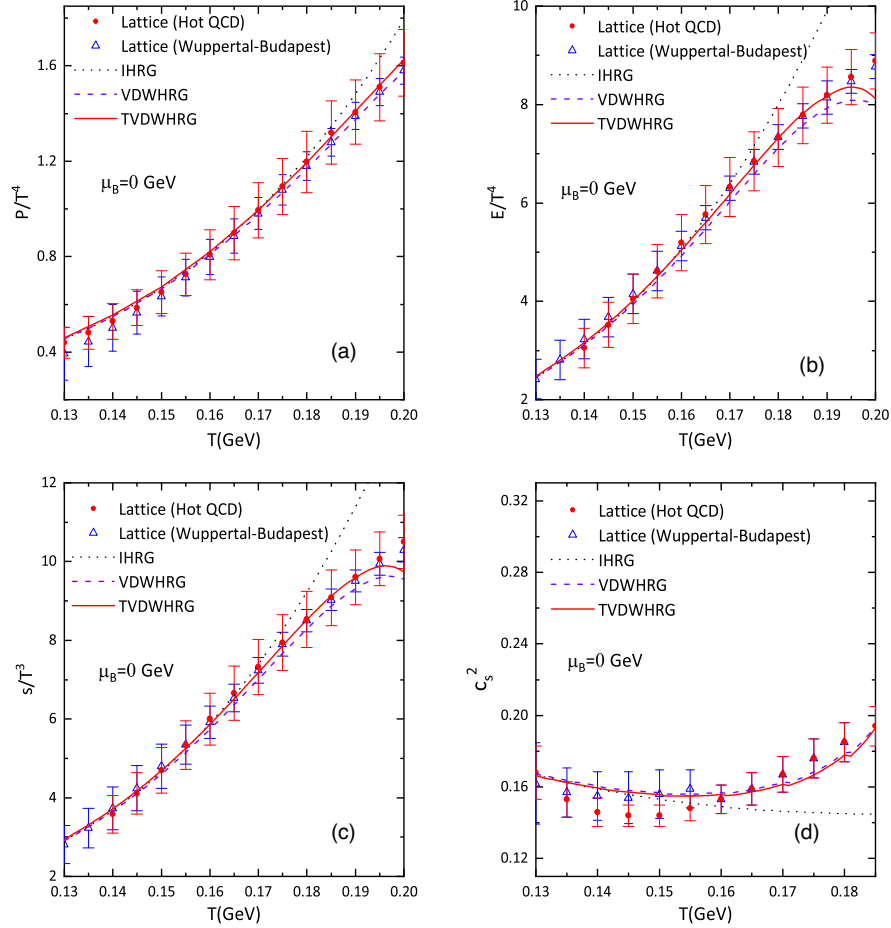


FIG. 3. The temperature dependences of the scaled pressure (a), scaled energy density (b), scaled entropy density (c) and square of the speed of sound (d) within IHRG model (black dashed lines), VDWHRG model (blue dashed lines), and TVDHRG model (red solid lines) at $\mu_B = 0$. The lattice QCD results are taken from the Wuppertal-Budapest [3] (red solid circle symbol with error bar) and HotQCD Collaborations [4] (blue up-triangle symbol with error bar).

$a \approx 239 \text{ MeV fm}^3$ and $b = \frac{4\pi r_n^3}{3} \approx 3.42 \text{ fm}^3$ (r_n is the radius of the nucleons) from fitting the properties of nuclear matter at zero temperature [72].

The temperature dependences of the scaled pressure P/T^4 , the scaled energy density ϵ/T^4 , the scaled entropy density s/T^3 , and speed of sound squared $c_s^2 = dP/d\epsilon$ at $\mu_B = 0 \text{ GeV}$ within the IHRG, VDWHRG, and TVDHRG models, respectively, are depicted in Fig. 3. It is noted that in Figs. 3(a)–3(c), comparing with the results in the IHRG model, the pressure, energy density, and entropy density within the VDWHRG and TVDHRG models has a modest suppression at $T > 0.16 \text{ GeV}$ due to the suppression of the number density of (anti)baryons in the medium. The scaled pressure P/T^4 , scaled energy density ϵ/T^4 , and scaled entropy density s/T^3 in the TVDHRG model have better agreement with the lattice QCD data of the Wuppertal-Budapest [3] and the Hot QCD Collaborations [4] up to $T = 0.195 \text{ GeV}$. The mild quantitative difference between these thermodynamics in the VDWHRG model and the counterparts in the TVDHRG

model at $T > 0.16 \text{ GeV}$ results from an enhancement factor of $\exp[-m(T, \mu_B)/T]$ with the decrease of the hadron masses in the TVDHRG model. In Fig. 3(d), we observe that the speed of sound squared c_s^2 in the TVDHRG model and VDWHRG model is consistent with the lattice QCD data at $T = 0.165\text{--}0.18 \text{ GeV}$. While c_s^2 within all considered HRG models, it gives a bad fit to the lattice QCD data of the Hot QCD Collaboration at $T = 0.135\text{--}0.155 \text{ GeV}$. In addition, the pressure, energy density, entropy density, and speed of sound squared are not sensitive to the choice of the considered HRG models at $T < 0.16 \text{ GeV}$. It can be explained in two aspects. (i) The VDW interactions between baryon-baryon pairs and between antibaryon-antibaryon pairs for $\mu_B = 0 \text{ GeV}$ are relatively weak at $T < 0.16 \text{ GeV}$ because at low T the contribution of the mesons is dominant in the system compared to the contribution of (anti)baryons. (ii) At $T < 0.16 \text{ GeV}$, the masses of the hadrons for $\mu_B = 0$ are nearly not affected by the temperature, as seen from Figs. 1 and 2.

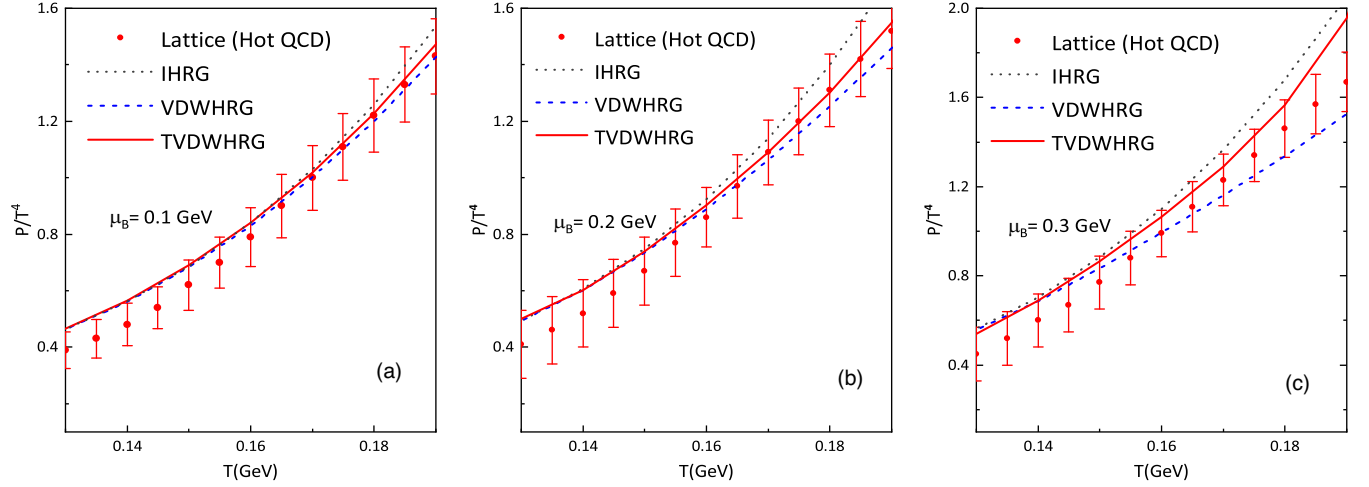


FIG. 4. The temperature dependence of the scaled pressure (P/T^4) within the IHRG model (dashed black lines), VDWHRG model (wide dashed purple lines), and TVDWHRG model (solid red lines) at $\mu_B = 0.1$ (a), 0.2 (b), and 0.3 GeV (c). The lattice QCD results (red symbol with error bar) are taken from Ref. [87].

Figures 4(a)–4(c) show the scaled pressure as a function of the temperature for $\mu_B = 0.1, 0.2,$ and 0.3 GeV. We see that the scaled pressure is underestimated by all models at $T < 0.16$ GeV. For the cases of $\mu_B = 0.1$ and 0.2 GeV, the scaled pressure within the TVDWHRG model fits better with the lattice QCD data at $T = 0.16$ – 0.19 GeV than that within the VDWHRG model or IHRG model. Compared to the VDWHRG model, the scaled pressure for zero and small μ_B (viz., $\mu_B = 0.1$ and 0.2 GeV) in the TVDWHRG model has a small quantitative enhancement. At higher μ_B (i.e., $\mu_B = 0.3$ GeV), we notice that the scaled pressure within the TVDWHRG model is significantly higher than that within the VDWHRG model, as shown in Fig. 4(c). This means that with the increase of μ_B , the effect of the thermal hadron masses on thermodynamics becomes more influential. However, the scaled pressure for $\mu_B = 0.3$ GeV fails to simulate the lattice QCD data within all considered HRG models. There are two possible reasons for the failure: (i) The parameters of the VDW model may vary with μ_B [65]. (ii) It is a challenging task for the lattice QCD simulation to give very reliable prediction of these quantities due to the so-called sign problem at nonzero μ_B . The lattice QCD data we used here are only estimated up to μ_B^2 [87]. Therefore, in the case of nonzero baryon chemical potential, we may not pay much attention to comparing our results with the lattice QCD data in precision; instead, we explore the effects of thermal hadron masses and VDW interactions on thermodynamic quantities and transport coefficients in hot hadronic matter.

The temperature dependence of the shear viscosity to entropy density ratio η/s within the TVDWHRG model at $\mu_B = 0$ GeV (purple solid line) is shown in Fig. 5. We can note that η/s decreases with increasing temperature, and the value of η/s within the TVDWHRG model meets the quantum lower bound $\eta/s = 1/4\pi$ proposed by Kovtun, Son, and Starinets (KSS) [88] in the vicinity of

$T = 0.17$ GeV. This means that the applicability of the TVDWHRG model should be restricted to the temperature domain in which $\eta/s > 1/4\pi$. At $\mu_B = 0.35$ GeV, our result of η/s (green dotted-dashed line) remains above the KSS bound in the entire temperature domain we considered here. We also notice that in the low T domain, η/s is slightly smaller at $\mu_B = 0.35$ GeV than at $\mu_B = 0$ GeV; however, in the high T domain, η/s is higher at $\mu_B = 0.35$ GeV than at $\mu_B = 0$ GeV. This behavior is also observed in Fig. 7 of Ref. [9] and in Fig. 6 of Ref. [89], and we will discuss this behavior later.

Figure 5 also demonstrates the comparison of our calculations with the results from other related models

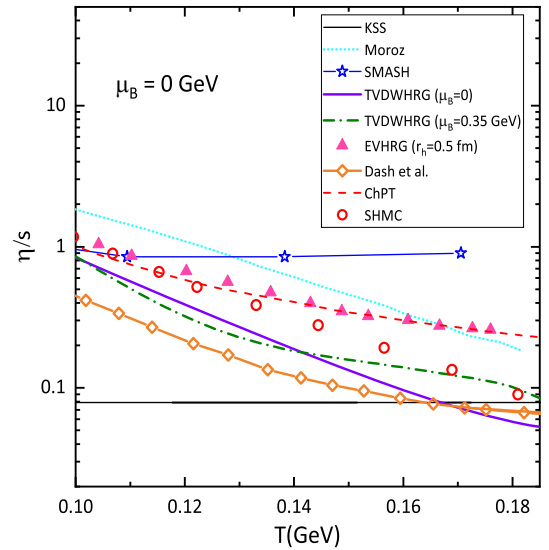


FIG. 5. Comparison of several calculations for the shear viscosity to entropy density ratio η/s at $\mu_B = 0$ GeV; see text for more explanations.

for $\mu_B = 0$ GeV. The open red circles correspond to the result of η/s for the hadron phase using the RTA within the SHMC model [35]. The blue star line corresponds to the result of η/s for hadron gas using the Kubo-Green formalism in the SMASH transport code [19]. The result of η/s by Dash *et al.* (orange diamond-dashed line) is computed in the framework of an S -matrix-based HRG model using the CE approximation and K -matrix cross sections [9]. The red dotted line represents the result of η/s using the Green-Kubo formalism in unitarized ChPT, which is a low-energy effective model of QCD describing the dynamics of the Nambu-Goldstone bosons [27]. The result of η/s by Moroz (cyan short dotted line) is obtained from solving the Boltzmann equation in the RTA, while the cross sections are extracted from UrQMD [16]. The pink triangles show the calculation of η/s for hadron gas in the EVHRG model [25]. All aforementioned works except the SMASH model give qualitative results which are similar to ours, although the exact magnitude of η/s differs in different model estimations. The result of Moroz [16] is about 3 times larger than ours, mainly due to the discrepancies in the cross sections. In Moroz's calculation, the cross sections extracted from the UrQMD model for different hadron-hadron elastic collisions are different, whereas an overall constant cross section is used in the current work. The SHMC result [35] is close to ours at $T < 0.12$ GeV and is about 2 times larger than our estimation at $T > 0.12$ GeV. This is mainly because although the hadron masses in the SHMC model and TVDWHRG model are in-medium dependent, the cross sections in the SHMC model are temperature dependent rather than a constant. The result of Dash *et al.* [9] is a factor of 2 smaller than ours at $T < 0.14$ GeV; however, as the temperature increases further, their result is very close to ours. The quantitative difference can be attributed to the uses of various approximation methods and cross sections. In our work, the transport coefficients are calculated in the RTA, which is different from the CE method. We emphasize that in the current work the cross sections are taken as constant, whose assumption could be improved in future studies. Furthermore, η/s calculated by Dash *et al.* also violates the KSS bound near the critical temperature taken from Ref. [90]. The estimation of η/s in SMASH [19] is close to ours at $T < 0.12$ GeV, while as the temperature increases, the SMASH result remains almost constant. This behavior can be explained as follows: First, in our work we only include elastic binary collisions between hadrons with constant cross sections, while the energy-dependent cross sections and hadron interactions dominated by resonance formation are included in SMASH. Second, the effect of resonance lifetimes on the relaxation time is considered in SMASH, whereas we use the thermal averaged relaxation time which contains no feedback from the resonance lifetimes (zero decay width used in our work for resonances). The result in the EVHRG model [25] and the

ChPT result [27] match well with ours at $T < 0.12$ GeV; however, their estimations are about 3 times larger than ours at high T . The numerical difference between the ChPT result and ours might be due to the fact that at high T more meson-baryon scatterings are included in the TVDWHRG model, while only $\pi - \pi$ scattering is considered in ChPT. The deviation between the estimation of η/s in the EVHRG model and ours at high T mainly arises from that, in Ref. [25] the authors consider that the repulsive interaction is related to all hadrons with the same radius ($r_h = 0.5$ fm), whereas in the TVDWHRG model, only VDW interactions between pairs of (anti)baryons are included, and all hadrons have the same radius as nucleons. Actually, the thermal mass effect on η/s is not obvious within the TVDWHRG model at zero μ_B or small μ_B , while as μ_B increases, this effect becomes more pronounced, which is shown in Fig. 7.

Here we refer to the hadron resonance gas model that only includes the effect of thermal hadron masses as the thermal HRG (THRG) model. To better understand how the effects of in-medium hadron masses and VDW interactions between (anti)baryons influence the transport coefficients in hadronic matter, we compute the variation of transport coefficients with T and μ_B in four HRG models: IHRG, THRG, VDWHRG, and TVDWHRG. The temperature dependence of the shear viscosity η at $\mu_B = 0.1, 0.2, 0.3, 0.35$ GeV for all considered HRG models is depicted in Fig. 6. We observe that η within the IHRG model increases monotonically as T increases at a fixed μ_B . This is because the variation of the shear viscosity η with T and μ_B in the IHRG model mainly comes from the number density in Eq. (42) rather than the relaxation time. Alternatively, at a given T the value of η in the IHRG model increases as μ_B grows. Considering the effect of thermal hadron masses, the value of η for $\mu_B = 0.1$ GeV within the THRG model has a mild enhancement in the relatively high T domain as shown in Fig. 6(a), which is similar to the result in Fig. 3(a) of Ref. [77]. This is due to the fact that the number density has an enhancement by considering the effect of thermal hadron masses. As μ_B increases, the improvement of η in the THRG model is more obvious than in the IHRG model, which arises because the positive effect of thermal hadron masses on the number density strengthens significantly with increasing μ_B . When the VDW interactions are taken into account in the estimation of η [as in Fig. 6(b)], η rises at a larger incremental rate at high temperature in the VDWHRG model as compared to the IHRG model. This can be interpreted as follows: First, at low T the dominant contributions to total η are light mesons which are nearly not affected by VDW interactions. Second, with increasing T , more and more baryons emerge in the system, and the baryon density can be suppressed in the VDWHRG model as compared to the IHRG model. However, the relaxation times for all hadrons in the VDWHRG model have a significant enhancement due to the scattering with baryons. As the temperature increases, the effect of a rapid rise in the

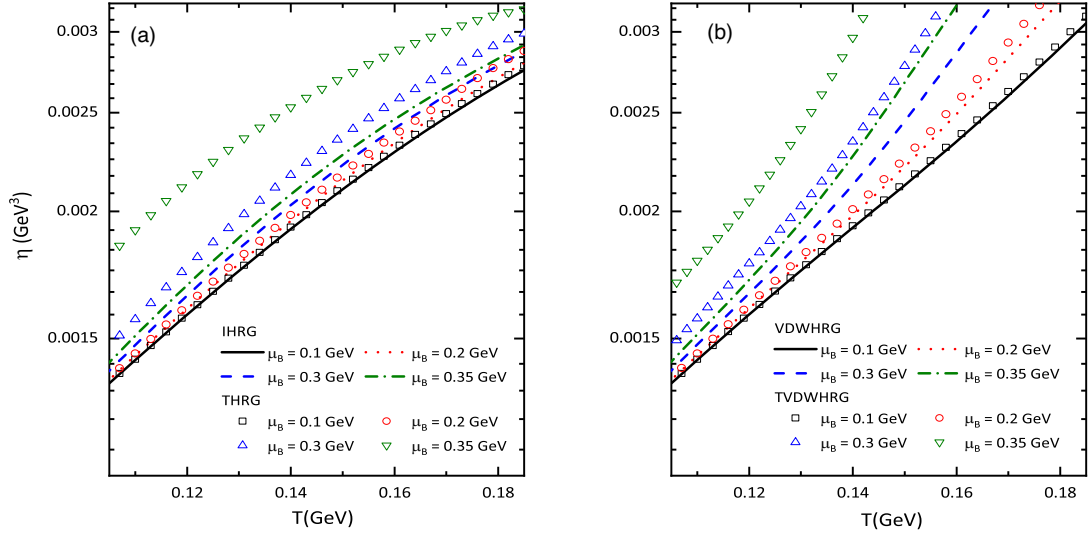


FIG. 6. Left panel (a) shows the temperature dependence of shear viscosity η within the IHRG (lines) and THRG (symbols) models for $\mu_B = 0.1$ GeV (black solid line and square symbol), 0.2 GeV (red dotted line and circular symbol), 0.3 GeV (blue dashed line and up-triangle symbol), and 0.35 GeV (green dashed-dotted line and down-triangle symbol). Right panel (b) shows the temperature dependence of η within the VDWHRG (lines) and TVDWHRG (symbols) models for $\mu_B = 0.1, 0.2, 0.3,$ and 0.35 GeV.

relaxation time wins over the impact of a fall in the number density within the VDWHRG model. Furthermore, we see that the evolution of η with μ_B in the VDWHRG model mimics that in the IHRG model. At high μ_B (viz., $\mu_B = 0.3$ or 0.35 GeV), considering simultaneously the effects of VDW interactions and in-medium hadron masses, the number density in the TVDWHRG model increases more sharply than that in the VDWHRG model, although the relaxation time in the TVDWHRG model is slightly reduced compared with that in the VDWHRG model. The final result of the interplay of the number density and the relaxation time in Eq. (42) shows the TVDWHRG model gives a further improvement in η compared to the VDWHRG model, as shown in Fig. 6(b).

Figure 7(a) presents our calculation of η/s for various μ_B in the IHRG and THRG models. We note that the T dependence of η/s within the IHRG and THRG models is mainly governed by the inverse entropy density $1/s$. The ratio η/s in the IHRG and THRG models decreases as T and μ_B increase solely due to the larger value of the entropy density for high T and high μ_B . Compared to the IHRG model, the THRG model leads to a suppression of η/s , which arises from the significant enhancement of the entropy density in the THRG model. At small μ_B ($\mu_B = 0.1$ and 0.2 GeV) or zero μ_B , η/s is nearly unaffected by the inclusion of in-medium hadron masses. The reasons are twofold. On the one hand, the effect of thermal hadron masses is weaker in the small μ_B case than in the high μ_B

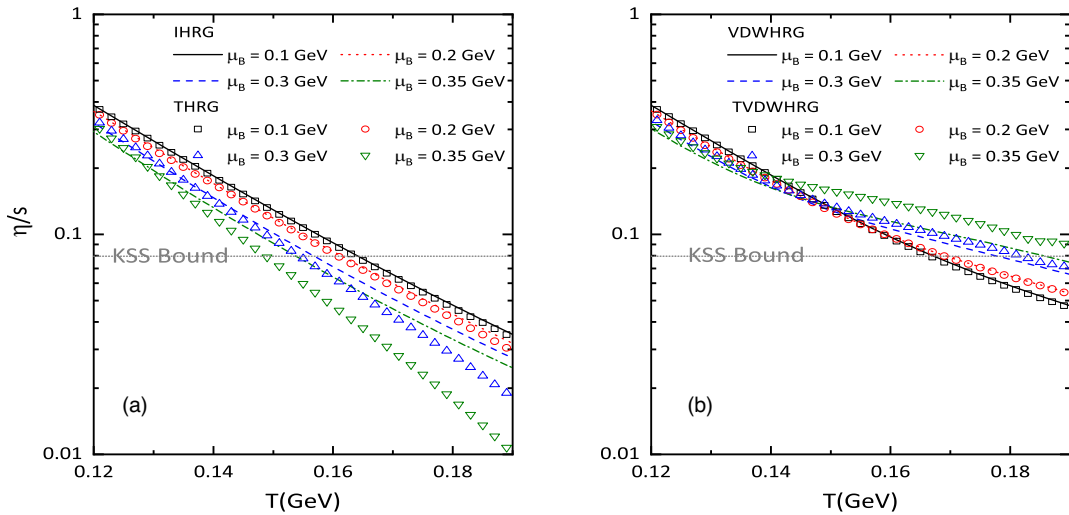


FIG. 7. Same as Fig. 6 for the ratio η/s . The gray dotted line is the KSS bound.

case. On the other hand, with the consideration of the thermal hadron masses, the increase in η is nearly neutralized by the decrease in $1/s$. Hence, from a quantitative aspect, the effect of the thermal hadron masses on η/s is important, especially at high μ_B .

Figure 7(b) displays η/s in the VDWHRG and TVDWHRG models as a function of the temperature at various μ_B . It is interesting to note that in the VDWHRG or TVDWHRG model, as μ_B grows η/s decreases at low T , whereas it increases at high T , which is qualitatively akin to the result of η/s in Ref. [89]. This nontrivial behavior of η/s in the VDWHRG model case is not observed in the EVHRG model [25]. The nonmonotonic variation of η/s with μ_B is because in the high T domain, as μ_B grows the rapid increase of η (as in Fig. 6) greatly overwhelms the decrease of $1/s$ in the VDWHRG model. Furthermore, at high μ_B (viz., $\mu_B = 0.3$ and 0.35 GeV), the effect of VDW interactions on η/s in the high T domain can be strengthened further by the inclusion of thermal hadron masses, even though thermal hadron masses themselves have a negative effect on η/s . Hence, the consideration of VDW interactions (thermal hadron masses) mainly changes qualitatively (quantitatively) the behavior of η/s . In Fig. 7(b), we also observe the location where $\eta/s(T, \mu_B) \simeq 1/4\pi$ shifts toward higher temperature with increasing μ_B in the TVDWHRG and VDWHRG models, contrary to the IHRG and THRG models case.

In regard to the scaled electrical conductivity σ_{el}/T at vanishing μ_B , we compare our result of the TVDWHRG model (olive-green solid line) with existing estimations, as shown in Fig. 8. The pink short dotted line represents the result for pion gas in the unitarized ChPT via the Green-Kubo technique [27]. The blue open triangles show the result obtained from the PHSD approach [41], which is a covariant extension to the Boltzmann-Uehling-Uhlenbeck approach [91] in the hadronic sector. The cyan solid squares represent the calculation of σ_{el}/T for hadronic gas employing SMASH using the Green-Kubo formalism [40]. The orange dotted-dashed line shows the result of the EVHRG model using the RTA [51]. The gray open circles show the computation of σ_{el}/T for $\pi - K - N$ gas in kinetic theory (KT) using a CE-like expansion of the distribution function [37]. The red full circles are the data from the $2 + 1$ flavor anisotropic lattice QCD calculation [43]. The black dashed line is the estimation of σ_{el}/T in a conformal super-Yang-Mills (SYM) theory [92]. In Ref. [39], Ghosh provided an estimation of σ_{el}/T for the $\pi - N$ system from electromagnetic current-current correlators in the static limits (brown stars). The bright green diamonds show the result of σ_{el}/T in the NJL model [30].

From Fig. 8, we notice that the variation of σ_{el}/T with the temperature in the Nambu-Jona-Lasinio (NJL) model and the KT and SYM theory is not obvious, and other model estimations and our result indicate that σ_{el}/T for $\mu_B = 0$ GeV significantly decreases at $T = 0.1$ – 0.18 GeV.

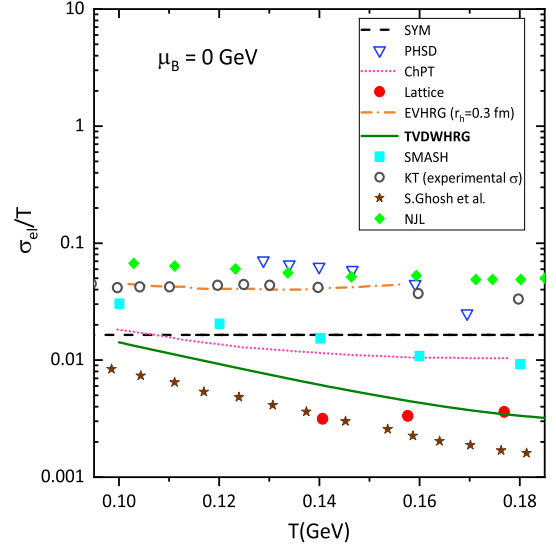


FIG. 8. Comparison of several calculations for the scaled electrical conductivity σ_{el}/T at $\mu_B = 0$ GeV; see text for more explanations.

The result of SMASH [40] is roughly 3 times larger than ours. This is mainly attributed to the choices of the calculation methodology and cross sections, as well as the lack of elastic collisions of some possible particle pairs (e.g., elastic $\pi^+\pi^+$ and $\pi^-\pi^-$) in SMASH. The ChPT result [27] is close to ours at $T < 0.14$ GeV; however, with increasing T , the ChPT result is a factor of 3 larger than ours. In the ChPT, the degrees of freedom are only mesons; thus, we deduce that the inclusion of more hadron species (baryons) may reduce the electrical conductivity of system. The results of the NJL model [30] and PHSD model [41] are much larger than ours. This great deviation may be due to the fact that the elementary degrees of freedom in the NJL model and PHSD model are (anti)quarks instead of hadrons. The significant numerical difference between the KT result [37] and ours mainly arises from the uncertainties in the realistic cross sections and the different choices of the hadron spectrum. The result of Ghosh [39] is a factor of 2 smaller than ours, which is mainly due to the differences in the inputs of the medium constituents and the relaxation times. The reason for the numerical difference between the estimation of σ_{el}/T in the EVHRG model [51] and ours is similar to what we discussed earlier about η/s . It is worth noting that at high T , our result is close to the lattice QCD data, though our model contains no quark-gluon degrees of freedom.

Figure 9 displays the variation of the scaled electrical conductivity σ_{el}/T with respect to the temperature at $\mu_B = 0.1, 0.2, 0.3,$ and 0.35 GeV in all considered HRG models. The T and μ_B dependence on the total electrical conductivity is basically coming from the number density and the relaxation time in Eq. (43). The number density is more dominating than the relaxation time in determining

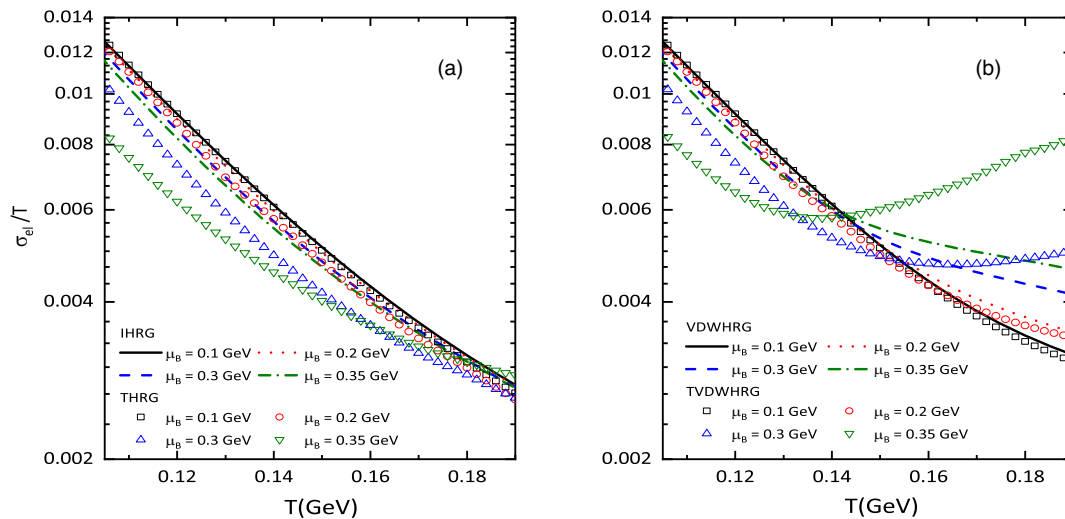


FIG. 9. Same as Fig. 6 for the scaled electrical conductivity σ_{el}/T .

the T and μ_B dependence on electrical conductivity for the baryonic contribution. However, for the mesonic contribution, the variation of the electrical conductivity in the IHRG model with T and μ_B is primarily governed by the relaxation time rather than the number density. This arises from the mathematical analysis of the electrical conductivities of mesons and baryons. As we can see from Fig. 9, the total σ_{el}/T in the IHRG model decreases as T increases for $\mu_B = 0.1$ GeV. One can understand this behavior as follows: First, the numerical strength of σ_{el}/T in the IHRG model mainly comes from the contribution of mesons. At a given μ_B , the contribution of the mesons to the total σ_{el}/T , σ_M/T decreases due to the decrease of the relaxation time via scattering with more hard spheres at high T . Second, the contribution of baryons to the total σ_{el}/T , σ_B/T increases as T grows, although the value of σ_B/T is very small compared to that of σ_M/T . Thus, after adding mesonic and baryonic contributions to the total σ_{el}/T , the qualitative behavior of the total σ_{el}/T in the IHRG model is still dominated by mesons (pions). With the increase of μ_B , the baryonic concentration increases and pions scatter with more baryons, leading to a reduction in the relaxation time of mesons. As a result, σ_M/T decreases with increasing μ_B . Although σ_B/T increases with growing μ_B , the increment in σ_B/T cannot win over the reduction in σ_M/T . Hence, the total σ_{el}/T in the IHRG model decreases with increasing μ_B , as shown in Fig. 9(a). Similar to shear viscosity, we also discuss the effects of in-medium hadron masses and VDW interactions on the total σ_{el}/T . As we can see from Fig. 9(a), at $\mu_B = 0.2$ GeV the value of the total σ_{el}/T is relatively smaller in the THRG model than in the IHRG model, which is mainly due to the reduction in the relaxation time of mesons within the THRG model, although σ_B/T within the THRG model has a slight cancellation effect on the decrease of σ_M/T . We notice that in Fig. 9(a) at $\mu_B = 0.1$ GeV or zero μ_B the effect of

thermal hadron masses on the total σ_{el}/T is negligible due to the small in-medium modification of masses, whereas with the further increase of μ_B , the negative impact of thermal hadron masses on the total σ_{el}/T becomes stronger. So at high μ_B , the effect of in-medium hadron masses on σ_{el}/T is significant and nonignorable. Nonetheless, the THRG model does not change the qualitative behavior of σ_{el}/T . Hence, we can deduce that the total σ_{el}/T in the IHRG and THRG models is still quantitatively and qualitatively dominated by mesonic contribution, i.e., σ_M/T .

Next we consider the effect of VDW interactions on the total σ_{el}/T . In Fig. 9(b), the total σ_{el}/T for $\mu_B = 0.1$ GeV is significantly enhanced at high T in the VDWHRG model compared to the IHRG model. The reasons are as follows: First, the increase in the relaxation time of mesons due to the inclusion of VDW interactions makes an enhancement in σ_M/T at high T . Second, compared to the IHRG model, the VDWHRG model leads to an improvement (reduction) in the relaxation time (the number density) of baryons at high T . And the strong rise in the relaxation time of baryons within the VDWHRG model makes σ_B/T have a large enhancement at high T after dominating over the decrease of the number density of baryons. Nevertheless, the total σ_{el}/T is still decreasing over the entire temperature domain in the VDWHRG model similar to that in the IHRG model. The dependence of σ_{el}/T on μ_B in the VDWHRG model is nonmonotonic, in stark contrast to that in the IHRG model, as shown in Fig. 9(b). More exact, as μ_B grows, the total σ_{el}/T in the VDWHRG model first decreases at low T then increases at high T . In order to better understand this nontrivial behavior, the temperature dependences of σ_B/T and σ_M/T within the VDWHRG model at various μ_B are plotted in Fig. 10(a). At high T , σ_B/T in the VDWHRG model is comparable to σ_M/T , and the increase of σ_B/T is enough to compensate for the inconspicuous decrease of σ_M/T with the increase in μ_B . Thus, at high temperature,

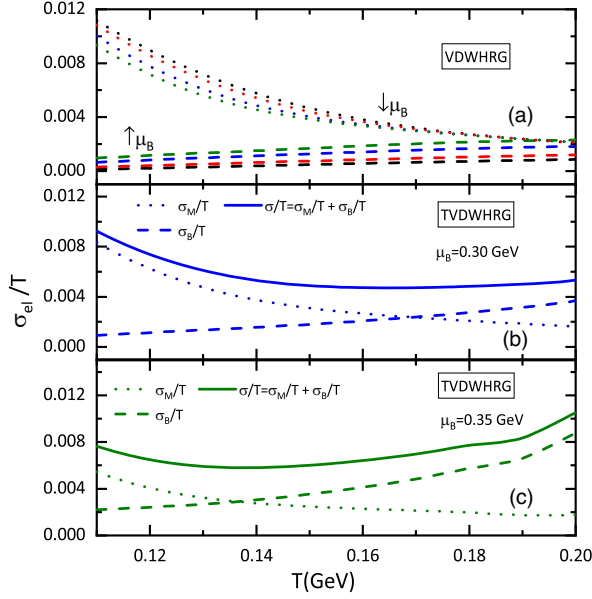


FIG. 10. The temperature dependence of the scaled electrical conductivity for meson (dotted lines) and baryon components (dashed lines), and their total (solid lines) at various μ_B .

the variation of the total σ_{el}/T with μ_B is dominated by σ_B/T , as shown in Fig. 10(a). We also study the mix effects of thermal hadron masses and VDW interactions on the total σ_{el}/T at various μ_B . In Fig. 9(b), we observe that the variation of the total σ_{el}/T with μ_B in the TVDWHRG model is analogous to that in the VDWHRG model. It is worth noting that σ_{el}/T in the TVDWHRG model at $\mu_B = 0.3$ and 0.35 GeV shows a broad hollow with a minimum, which is qualitatively similar to the result in Ref. [39], where σ_{el}/T for the $\pi - N$ system is calculated at $\mu_N = 0.4, 0.5,$ and 0.6 GeV. Similarly, the results in the PHSD model [42] and NJL model [30] show that σ_{el}/T at $\mu_B = 0$ GeV decreases in the hadronic temperature region but increases in the partonic temperature region and the minimum of σ_{el}/T around the critical temperature. This nonmonotonic behavior of σ_{el}/T is because the value of σ_B/T for $\mu_B = 0.3$ and 0.35 GeV in the TVDWHRG model significantly overshoots the value of σ_M/T at high T , as shown in Figs. 10(b) and 10(c). Therefore, we conclude that at high μ_B the positive effect of the VDW interactions on electrical conductivity will be further improved by the inclusion of thermal hadron masses, even if the thermal mass effect itself leads to a reduction in electrical conductivity.

Figure 11 displays the temperature dependence of the scaled thermal conductivity λ/T^2 within the TVDWHRG model at $\mu_B = 0.1$ GeV (black solid line). We remind the reader that in a baryon-free ($n_B = 0$) hadronic system, there is no thermal conduction which is related to the relative flow of energy and baryon number; hence, thermal conductivity vanishes. But for pure pion gas with conserved number, thermal conductivity can be nonzero at vanishing μ_B [14]. We also compare our result with the results of

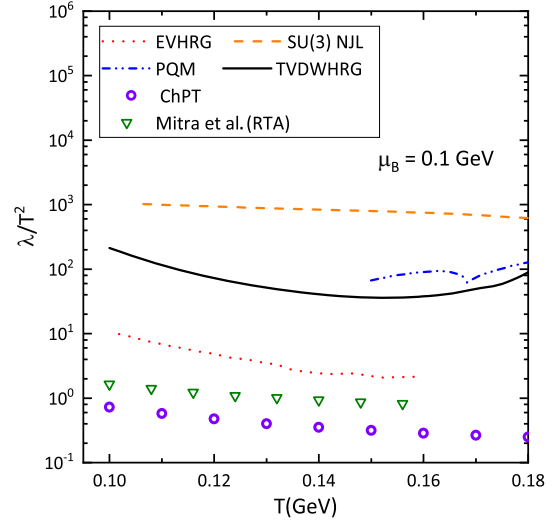
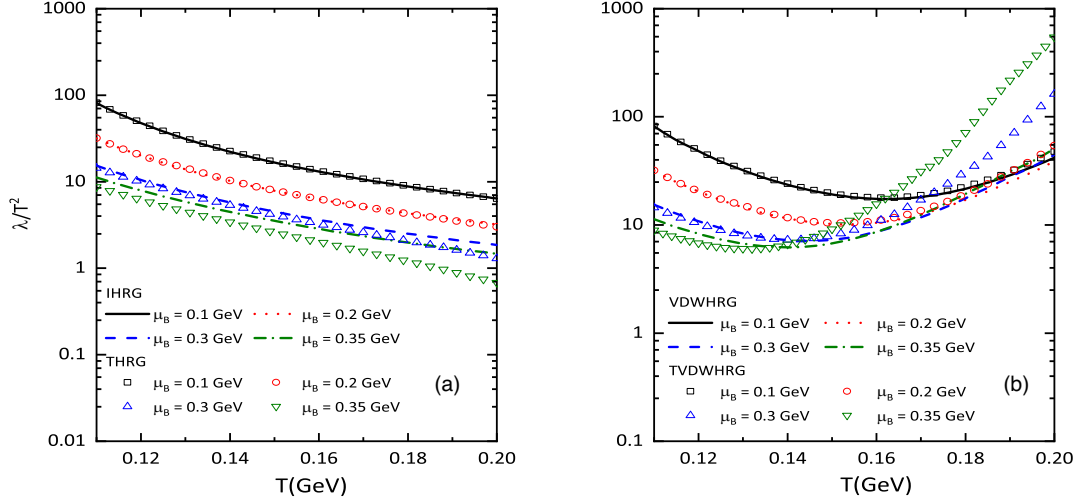


FIG. 11. Comparison of several calculations for the scaled thermal conductivity λ/T^2 at $\mu_B = 0.1$ GeV; see text for more explanations.

some earlier works. The orange dashed line and blue double-dotted-dashed line correspond to the estimation of λ/T^2 at $\mu_B = 0.1$ GeV in the SU(3) NJL model [30] and in the SU(2) Polyakov quark meson (PQM) model [32], respectively. The red dotted line represents the result of the EVHRG model [51]. The green triangles represent the estimation of λ/T^2 by Mitra and Sarkar for pion gas using the RTA [45]. The purple open circles show the result for pion gas in unitarized ChPT using the Green-Kubo formalism [27]. We notice our result is more or less qualitatively similar to these existing results, whereas the calculations of various models have significantly different orders of magnitude. The estimation of λ/T^2 by Mitra and Sarkar [45] and the ChPT result [27] are far less than ours, since the total λ/T^2 in pion gas is only coming from $\pi - \pi$ elastic scatterings. The numerical difference between the result of the EVHRG model and our result may again be attributed to the fact that in Ref. [51] the repulsive interactions are related to all hadrons rather than only baryon-baryon pairs and antibaryon-antibaryon pairs. In addition, the results of λ/T^2 in the NJL [30] and PQM models [32] are larger than ours since the elementary degrees of freedom in the NJL model (PQM model) are quarks (quarks and light mesons), whereas the degrees of freedom in the HRG models are hadrons.

The temperature dependence of λ/T^2 for $\mu_B = 0.1, 0.2, 0.3, 0.35$ GeV within all considered HRG models is plotted in Fig. 12. At a given μ_B , the monotonically decreasing behavior of λ/T^2 in the IHRG model is in large part qualitatively determined by the heat function w/n_B as shown in Eq. (44). Furthermore, at a given temperature, λ/T^2 decreases as μ_B increases within the IHRG model. This mainly arises from the baryon density n_B increasing by the significant amount with increasing μ_B ; although the


 FIG. 12. Same as Fig. 6 for the scaled thermal conductivity λ/T^2 .

enthalpy density w also increases as μ_B grows, this effect is small. In Fig. 12(a), for high μ_B (viz., $\mu_B = 0.3$ and 0.35 GeV), λ/T^2 in the THRG model is reduced quantitatively compared to that in the IHRG model. This is because although the values of both w and n_B have an enhancement by the inclusion of in-medium hadron masses, the enhancement of n_B is so large that w/n_B in the THRG model as a whole has a reduction compared to that in the IHRG model. At small μ_B ($\mu_B = 0.1$ and 0.2 GeV) or zero μ_B , λ/T^2 is nearly unaffected by the inclusion of in-medium hadron masses. This is mainly because, with the consideration of thermal hadron masses, the increase in n_B is nearly neutralized by the decrease in $1/w$. Hence, the in-medium hadron masses play an important role in the calculation of λ/T^2 , especially at high μ_B .

We observe that the qualitative variation of λ/T^2 with T and μ_B in the THRG model is akin to that in the IHRG model, as shown in Fig. 12(a). However, when we consider the effect of VDW interactions on λ/T^2 , its behavior becomes unusual. In Fig. 12(b), λ/T^2 for $\mu_B = 0.1$ GeV in the VDWHRG model first decreases, reaches a minimum, and then increases with increasing temperature, which is not observed in the EVHRG model [51], and the minimum of λ/T^2 for $\mu_B = 0.1$ GeV is around $T = 0.16$ GeV. Similarly, λ/T^2 in the PQM model [32] and NJL model [93] for $\mu_B = 0.1$ GeV also shows a nonmonotonic behavior with a minimum near the critical temperature. This valley structure of λ/T^2 in the VDWHRG model may be explained as follows: At low T , the hadronic system is dominated by light mesons whose contributions to λ/T^2 are nearly not affected by VDW interactions. Thus, at low T , the T and μ_B dependence on λ/T^2 in the VDWHRG model mimics that in the IHRG model. With increasing T , the baryonic states increase, and the VDW interactions lead to a reduction in both w and n_B ; however, the reduction of n_B is so prominent that it makes

λ/T^2 an increasing function of T in the high T domain. In short, the μ_B dependence on λ/T^2 in the VDWHRG model is still analogous to that in the THRG and IHRG models. We also notice that the minimum of λ/T^2 in the VDWHRG model shifts to a lower temperature as μ_B increases. Furthermore, the effect of the VDW interactions on λ/T^2 is more pronounced by the inclusion of thermal hadron masses at high μ_B ($\mu_B = 0.3$ and 0.35 GeV), even though the effect of thermal masses themselves can result in a numerical decrease of λ/T^2 . Thus, for $\mu_B = 0.3$ and

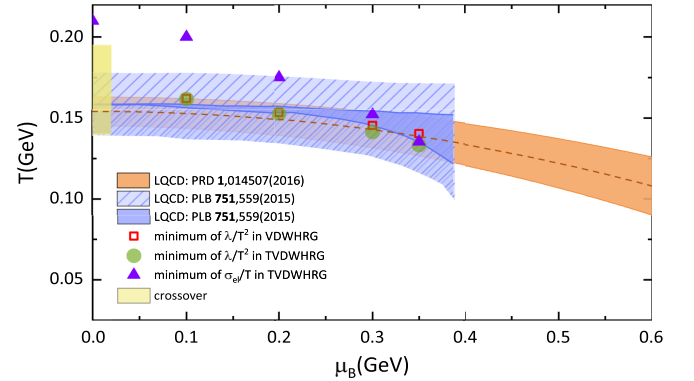


FIG. 13. The minima for σ_{el}/T in the VDWHRG model (purple solid triangles) and minima for λ/T^2 in the VDWHRG model (orange open squares) and TVDWHRG model (green solid circles) in the $T - \mu_B$ plane. The phase diagram obtained by analytic continuation of lattice QCD simulations from imaginary to real μ_B [94,95]. The blue dashed band and orange solid band indicate the width of the phase transition. The blue solid band is the critical line from Ref. [95]. The widening around 0.3 GeV is coming from the uncertainty of the curvature and from the contribution of higher order. The orange dashed line shows the transition line from Ref. [94]. The yellow band is the expected crossover region ($T = 0.14 - 0.19$ GeV) for $\mu_B = 0$ GeV in Ref. [2].

0.35 GeV, λ/T^2 in the TVDWHRG model increases faster at high T compared to that in the VDWHRG model, and the value of λ/T^2 at $\mu_B = 0.35$ GeV even overshoots the value of λ/T^2 at $\mu_B = 0.3$ GeV, which can be shown in Fig. 12(b).

Figure 13 shows the minima of σ_{el}/T for the TVDWHRG model and the minima of λ/T^2 for the VDWHRG and TVDWHRG models in the $T - \mu_B$ plane. We notice that these minima are phenomenologically located inside or slightly deviate the phase transition region obtained from lattice QCD simulations [94,95]. For λ/T^2 , the minima in the VDWHRG and TVDWHRG models are very close to the critical transition lines. Based on previous results in Refs [30,42,49,93] where the minimum of σ_{el}/T (λ/T^2) is near the critical temperature at $\mu_B = 0$ GeV ($\mu_B = 0.1$ GeV), we expect the scaled electrical and thermal conductivities in the TVDWHRG model at different μ_B to exhibit a minimum near the QGP-hadron phase transition region making it a crucial signature of the phase transition. To our knowledge, there are no results of the scaled conductivities based on lattice QCD calculations and the effective QCD models at different nonzero μ_B , so whether the minimum is really a sign of a phase transition still needs to be verified in the future.

VI. CONCLUSION

In this work, we investigate the thermodynamics and transport coefficients with the TVDWHRG model, which is the extension of the VDWHRG model by including the effect of the temperature T - and baryon chemical potential μ_B -dependent hadron masses. In the TVDWHRG model, thermal hadron masses are obtained by the 2 + 1 flavor Polyakov linear sigma model combined with the scaling rule of hadron masses. We estimate the thermodynamics, such as the pressure, energy density, entropy density, and square of sound velocity in the TVDWHRG model and compare them with the lattice QCD data. We show that at $T \sim 0.16\text{--}0.195$ GeV, the thermodynamics for $\mu_B = 0$ GeV in the TVDWHRG model gives an improved agreement with the available lattice QCD data compared to that in the VDWHRG model. And with the increase of μ_B , the thermodynamics, e.g., the pressure, have a sizable improvement in magnitude due to the inclusion of thermal hadron masses.

We also investigate the scaled transport coefficients, such as the shear viscosity to entropy density ratio η/s , scaled electrical conductivity σ_{el}/T , and scaled thermal conductivity λ/T^2 of hadronic matter in all considered HRG models by using the quasiparticle kinetic theory under the

relaxation time approximation. From the qualitative and quantitative perspectives, taking into account the effects of VDW interactions and thermal hadron masses, the scaled transport coefficients are modified considerably. When we only consider the effect of T - and μ_B -dependent hadron masses compared to the IHRG model case, the values of all scaled transport coefficients for fixed μ_B are relatively suppressed in the THRG model even though η itself is enhanced in the THRG model. Though the suppression of the scaled transport coefficients due to the thermal mass effect is relatively weak at small μ_B (viz., $\mu_B = 0, 0.1, 0.2$ GeV), with the increase of μ_B its effect becomes more pronounced. Nonetheless, the general behaviors of the transport coefficients in the THRG and IHRG models are similar qualitatively.

However, compared to the IHRG model, the VDWHRG model leads to a qualitatively and quantitatively different behavior of the scaled transport coefficients. On the one hand, the VDW interactions between (anti)baryons give a significant enhancement of the scaled transport coefficients at high T and even change the dependence of λ/T^2 on the temperature. On the other hand, as μ_B grows, η/s and σ_{el}/T in the VDWHRG or TVDWHRG model decrease at low T , whereas they increase at high T . Furthermore, the effect of VDW interactions on the scaled transport coefficients for $\mu_B > 0.2$ GeV is strengthened further at high T by the inclusion of in-medium hadron masses, though thermal hadron masses themselves have a negative effect on the scaled transport coefficients. The minimum of σ_{el}/T in the TVDWHRG model and the minimum of λ/T^2 in the TVDWHRG or VDWHRG model may be related to the phase transition, which needs to be verified based on the research from different effective models. It is noted that we make some simple assumptions in the present TVDWHRG model, and there is much room for further improvement (e.g., the approaches we obtain all in-medium hadron masses could be improved, the VDW parameters may vary with μ_B , the quantitative changes of the constituent quark masses in various effective QCD models may be modified, etc.). However, we expect the improved TVDWHRG model does not break down the existing qualitative behaviors for the scaled transport coefficients in the present TVDWHRG model.

ACKNOWLEDGMENTS

This research is supported in part by the National Natural Science Foundation of China (NSFC) Project No. 11935007.

- [1] M. Cheng *et al.*, *Phys. Rev. D* **74**, 054507 (2006).
- [2] Y. Aoki, Z. Fodor, S. D. Katz, and K. K. Szabo, *Phys. Lett. B* **643**, 46 (2006).
- [3] S. Borsanyi, Z. Fodor, C. Hoelbling, S. D. Katz, S. Krieg, and K. K. Szabo, *Phys. Lett. B* **730**, 99 (2014).
- [4] Bazavov *et al.*, *Phys. Rev. D* **90**, 094503 (2014).
- [5] R. Bellwied, S. Borsanyi, Z. Fodor, S. D. Katz, and C. Ratti, *Phys. Rev. Lett.* **111**, 202302 (2013).
- [6] V. Vovchenko, M. I. Gorenstein, and H. Stoecker, *Phys. Rev. Lett.* **118**, 182301 (2017).
- [7] V. Vovchenko, *Phys. Rev. C* **96**, 015206 (2017).
- [8] S. Plumari, A. Paglisi, F. Scardina, and V. Greco, *Phys. Rev. C* **86**, 054902 (2012).
- [9] A. Dash, S. Samanta, and B. Mohanty, *Phys. Rev. D* **100**, 014025 (2019).
- [10] A. Wiranata, V. Koch, M. Prakash, and X. N. Wang, *Phys. Rev. C* **88**, 044917 (2013).
- [11] G. S. Denicol, C. Gale, S. Jeon, and J. Noronha, *Phys. Rev. C* **88**, 064901 (2013).
- [12] M. Prakash, M. Prakash, R. Venugopalan, and G. Welke, *Phys. Rep.* **227**, 321 (1993).
- [13] S. Mitra, U. Gangopadhyaya, and S. Sarkar, *Phys. Rev. D* **87**, 094026 (2013).
- [14] S. Gavin, *Nucl. Phys. A* **435**, 826 (1985).
- [15] G. Kadam, S. Pawar, and H. Mishra, *J. Phys. G* **46**, 015102 (2019).
- [16] O. N. Moroz, [arXiv:1301.6670](https://arxiv.org/abs/1301.6670).
- [17] U. Gangopadhyaya, S. Ghosh, S. Sarkar, and S. Mitra, *Phys. Rev. C* **94**, 044914 (2016).
- [18] S. Sarkar, *Adv. High Energy Phys.* **2013**, 627137 (2013).
- [19] J.-B. Rose, J. M. Torres-Rincon, A. Schäfer, D. R. Oliinychenko, and H. Petersen, *Phys. Rev. C* **97**, 055204 (2018).
- [20] N. Demir and S. A. Bass, *Phys. Rev. Lett.* **102**, 172302 (2009).
- [21] S. Pratt, A. Baez, and J. Kim, *Phys. Rev. C* **95**, 024901 (2017).
- [22] V. Ozvenchuk, O. Linnyk, M. I. Gorenstein, E. L. Bratkovskaya, and W. Cassing, *Phys. Rev. C* **87**, 064903 (2013).
- [23] J. Noronha-Hostler, J. Noronha, and C. Greiner, *Phys. Rev. Lett.* **103**, 172302 (2009); *Phys. Rev. C* **86**, 024913 (2012).
- [24] M. I. Gorenstein, M. Hauer, and O. N. Moroz, *Phys. Rev. C* **77**, 024911 (2008).
- [25] G. P. Kadam and H. Mishra, *Phys. Rev. C* **92**, 035203 (2015).
- [26] J. W. Chen and E. Nakano, *Phys. Lett. B* **647**, 371 (2007).
- [27] D. Fernandez-Fraile and A. Gomez Nicola, *Eur. Phys. J. C* **62**, 37 (2009).
- [28] P. Gerber and H. Leutwyler, *Nucl. Phys. B* **321**, 387 (1989).
- [29] S. Ghosh, F. E. Serna, A. Abhishek, G. Krein, and H. Mishra, *Phys. Rev. D* **99**, 014004 (2019).
- [30] R. Marty, E. Bratkovskaya, W. Cassing, J. Aichelin, and H. Berrehrh, *Phys. Rev. C* **88**, 045204 (2013).
- [31] A. N. Tawfik, A. M. Diab, and M. T. Hussein, *Int. J. Mod. Phys. A* **31**, 1650175 (2016).
- [32] P. Singha, A. Abhishek, G. Kadam, S. Ghosh, and H. Mishra, *J. Phys. G* **46**, 015201 (2019).
- [33] P. Chakraborty and J. I. Kapusta, *Phys. Rev. C* **83**, 014906 (2011).
- [34] M. Albright and J. I. Kapusta, *Phys. Rev. C* **93**, 014903 (2016).
- [35] A. S. Khvorostukhin, V. D. Toneev, and D. N. Voskresensky, *Nucl. Phys. A* **845**, 106 (2010).
- [36] S. Ghosh, S. Mitra, and S. Sarkar, *Nucl. Phys. A* **969**, 237 (2018).
- [37] M. Greif, C. Greiner, and G. S. Denicol, *Phys. Rev. D* **93**, 096012 (2016); **96**, 059902(E) (2017).
- [38] A. Puglisi, S. Plumari, and V. Greco, *Phys. Rev. D* **90**, 114009 (2014).
- [39] S. Ghosh, *Phys. Rev. D* **95**, 036018 (2017).
- [40] J. Hammelmann, J. M. Torres-Rincon, J. B. Rose, M. Greif, and H. Elfner, *Phys. Rev. D* **99**, 076015 (2019).
- [41] T. Steinert and W. Cassing, *Phys. Rev. C* **89**, 035203 (2014).
- [42] W. Cassing, O. Linnyk, T. Steinert, and V. Ozvenchuk, *Phys. Rev. Lett.* **110**, 182301 (2013).
- [43] G. Aarts, C. Allton, A. Amato, P. Giudice, S. Hands, and J. I. Skullerud, *J. High Energy Phys.* **02** (2015) 186.
- [44] S. Ghosh, *Int. J. Mod. Phys. E* **24**, 1550058 (2015).
- [45] S. Mitra and S. Sarkar, *Phys. Rev. D* **89**, 054013 (2014).
- [46] D. Davesne, *Phys. Rev. C* **53**, 3069 (1996).
- [47] U. Gangopadhyaya, S. Ghosh, and S. Sarkar, *Int. J. Mod. Phys. E* **28**, 1950035 (2019).
- [48] M. Braby, J. Chao, and T. Schäfer, *Phys. Rev. C* **81**, 045205 (2010).
- [49] A. Abhishek, H. Mishra, and S. Ghosh, *Phys. Rev. D* **97**, 014005 (2018).
- [50] A. Harutyunyan, D. H. Rischke, and A. Sedrakian, *Phys. Rev. D* **95**, 114021 (2017).
- [51] G. P. Kadam, H. Mishra, and L. Thakur, *Phys. Rev. D* **98**, 114001 (2018).
- [52] H. Satz, *Lect. Notes Phys.* **841**, 1 (2012).
- [53] H. Meyer-Ortmanns, *Rev. Mod. Phys.* **68**, 473 (1996).
- [54] D. H. Rischke, *Prog. Part. Nucl. Phys.* **52**, 197 (2004).
- [55] P. Costa, C. A. de Sousa, and Yu. L. Kalinovsky, *Phys. Rev. C* **70**, 025204 (2004); *Phys. Lett. B* **560**, 171 (2003).
- [56] P. Costa, M. C. Ruivo, C. A. de Sousa, H. Hansen, and W. M. Alberico, *Phys. Rev. D* **79**, 116003 (2009).
- [57] A. N. Tawfik, A. M. Diab, and M. T. Hussein, *Chin. Phys. C* **43**, 034103 (2019).
- [58] A. N. Tawfik and N. Magdy, *Phys. Rev. C* **91**, 015206 (2015).
- [59] V. K. Tiwari, *Phys. Rev. D* **88**, 074017 (2013).
- [60] A. N. Tawfik and A. M. Diab, *Phys. Rev. C* **91**, 015204 (2015).
- [61] H. Mao, J. Jin, and M. Huang, *J. Phys. G* **37**, 035001 (2010).
- [62] A. Andronic, P. Braun-Munzinger, J. Stachel, and M. Winn, *Phys. Lett. B* **718**, 80 (2012).
- [63] A. Baran, W. Broniowski, and W. Florkowski, *Acta Phys. Pol. B* **35**, 779 (2004).
- [64] R. K. Mohapatra, H. Mishra, S. Dash, and B. K. Nandi, [arXiv:1901.07238](https://arxiv.org/abs/1901.07238).
- [65] N. Sarkar and P. Ghosh, *Phys. Rev. C* **98**, 014907 (2018).
- [66] W. Greiner, L. Neise, and H. Stoecker, *Thermodynamics and Statistical Mechanics* (Springer-Verlag, New York, 1995).
- [67] N. F. Carnahan and K. E. Starling, *J. Chem. Phys.* **51**, 635 (1969).
- [68] S. Samanta and B. Mohanty, *Phys. Rev. C* **97**, 015201 (2018).

- [69] O. Redlich and J. N. S. Kwong, *Chem. Rev.* **44**, 233 (1949).
- [70] D. Y. Peng and D. Robinson, *Ind. Eng. Chem. Fundam.* **15**, 59 (1976).
- [71] H. A. Bethe, *Annu. Rev. Nucl. Part. Sci.* **21**, 93 (1971).
- [72] V. Vovchenko, D. V. Anchishkin, and M. I. Gorenstein, *J. Phys. A* **48**, 305001 (2015).
- [73] B. J. Schaefer and M. Wagner, *Phys. Rev. D* **79**, 014018 (2009).
- [74] A. M. Polyakov, *Phys. Lett.* **72B**, 477 (1978).
- [75] C. Ratti, M. A. Thaler, and W. Weise, *Phys. Rev. D* **73**, 014019 (2006).
- [76] P. Kovacs and Z. Szep, *Phys. Rev. D* **75**, 025015 (2007).
- [77] G. P. Kadam and H. Mishra, *Phys. Rev. C* **93**, 025205 (2016).
- [78] S. Leupold, *J. Phys. G* **32**, 2199 (2006).
- [79] J. Jankowski, D. Blaschke, and M. Spalinski, *Phys. Rev. D* **87**, 105018 (2013).
- [80] D. Blaschke, J. Berdermann, J. Cleymans, and K. Redlich, *Few Body Syst.* **53**, 99 (2012).
- [81] D. Blaschke, A. Dubinin, and L. Turko, *Phys. Part. Nucl.* **46**, 732 (2015).
- [82] P. Chakraborty and J. I. Kapusta, *Phys. Rev. C* **83**, 014906 (2011).
- [83] S. Mitra and V. Chandra, *Phys. Rev. D* **97**, 034032 (2018).
- [84] A. Wiranata and M. Prakash, *Phys. Rev. C* **85**, 054908 (2012).
- [85] M. E. Peskin and D. V. Schroeder, *An Introduction to Quantum Field Theory* (CRC Press, Boca Raton, 1995).
- [86] K. A. Olive *et al.* (Particle Data Group), *Chin. Phys. C* **38**, 090001 (2014).
- [87] S. Borsanyi, G. Endrodi, Z. Fodor, S. D. Katz, S. Krieg, C. Ratti, and K. K. Szabo, *J. High Energy Phys.* **08** (2012) 053.
- [88] P. Kovtun, D. T. Son, and A. O. Starinets, *Phys. Rev. Lett.* **94**, 111601 (2005).
- [89] S. Ghosh, *Braz. J. Phys.* **45**, 687 (2015).
- [90] A. Bazavov *et al.*, *Phys. Rev. D* **85**, 054503 (2012).
- [91] W. Cassing, V. Metag, U. Mosel, and K. Niita, *Phys. Rep.* **188**, 363 (1990).
- [92] S. Caron-Huot, P. Kovtun, G. D. Moore, A. Starinets, and L. G. Yaffe, *J. High Energy Phys.* **12** (2006) 015.
- [93] P. Deb, G. P. Kadam, and H. Mishra, *Phys. Rev. D* **94**, 094002 (2016).
- [94] P. Cea, L. Cosmai, and A. Papa, *Phys. Rev. D* **93**, 014507 (2016).
- [95] R. Bellwied, S. Borsanyi, Z. Fodor, J. Günther, S. D. Katz, C. Ratti, and K. K. Szabo, *Phys. Lett. B* **751**, 559 (2015).